IEEE Access
Multidisciplinary | Rapid Review | Open Access Journal

Received August 15, 2018, accepted October 5, 2018, date of publication October 18, 2018, date of current version November 9, 2018.

Digital Object Identifier 10.1109/ACCESS.2018.2876034

An Accurate and Efficient Device-Free Localization Approach Based on Sparse Coding in Subspace

HUAKUN HUANG[1], HAOLI ZHAO[1], XIANG LI[1], SHUXUE DING[1], (Member, IEEE), LINGJUN ZHAO[1], AND ZHENNI LI[2]

[1]School of Computer Science and Engineering, The University of Aizu, Aizuwakamatsu 965-0005, Japan
[2]School of Automation, Guangdong Key Laboratory of IoT Information Technology, Guangdong University of Technology, Guangzhou 510006, China

Corresponding author: Shuxue Ding (sding@u-aizu.ac.jp)

This work was supported by Grants-In-Aid for Scientific Research, Ministry of Education, Culture, Sports, Science, and Technology, Japan, under Grant 16K00335.

ABSTRACT In practical device-free localization (DFL) applications, for enlarging the monitoring area and improving localization accuracy, too many nodes need to be deployed, which results in a large volume of DFL data with high dimensions. This arises a key problem of seeking an accurate and efficient approach for DFL. In order to address this problem, this paper regards DFL as a problem of sparse-representation-based classification; builds a sparse model; and then proposes two sparse-coding-based algorithms. The first algorithm, sparse coding via the iterative shrinkage-thresholding algorithm (SC-ISTA), is efficient for handling high-dimensional data. And then, subspace techniques are further utilized, followed by performing sparse coding in the low-dimensional signal subspace, which leads to the second algorithm termed subspace-based SC-ISTA (SSC-ISTA). Experiments with the real-world data set are conducted for single-target and multi-target localization, and three typical machine learning algorithms, deep learning based on autoencoder, K-nearest neighbor, and orthogonal matching pursuit, are compared. Experimental results show that both SC-ISTA and SSC-ISTA can achieve high localization accuracies of 100% and are robust to noisy data when SNR is greater than 10 dB, and the time costs for sparse coding of SC-ISTA and SSC-ISTA are 2.1×10^{-3} s and 2.1×10^{-4} s respectively, which indicates that the proposed algorithms outperform the other three ones.

INDEX TERMS Device-free localization, wireless sensor networks, multi-targets, sparse coding, subspace, iterative shrinkage-thresholding algorithm.

I. INTRODUCTION

Wireless localization market has spawned extensive applications in Smart Cities, such as healthcare at home or in the hospitals [1], [2] (e.g., for detecting locations and activities of old people and patients), location-based services in smart spaces [3] (airports, shopping centers, touristic sites etc.), emergency rescue [4] (e.g., location detection of firefighters and survivors in the fire), indoor environment monitoring and control for energy saving in building [5], as well as for detecting and tracking intruder's location in security safeguard.

To support these scenarios mentioned above, various wireless localization techniques have been developed, e.g., GPS [6], infrared [7], ultrasound [8], and radio-frequency identification [9]. While applying the current techniques, the target must be equipped with a wireless device, such as smartphone, badge with a unique identifier code, ultrasonic receiver node, tags [10], [11]. However, these mentioned techniques may not be applicable to some scenarios. For example, for detecting intruders, or tracking people inside a building during a fire emergency, one cannot usually assume any pre-installed trackable devices on the targets.

Therefore, as an emerging technology, a device-free localization (DFL), using radio frequency (RF) sensor networks to detect, track and locate targets who do not carry any attached devices, has attracted tremendous interest recently [12]–[14]. As shown in Fig. 1, in a DFL system, wireless sensor nodes, which are normally termed as anchor points (AP), are used to sense targets by transmitting in some APs and

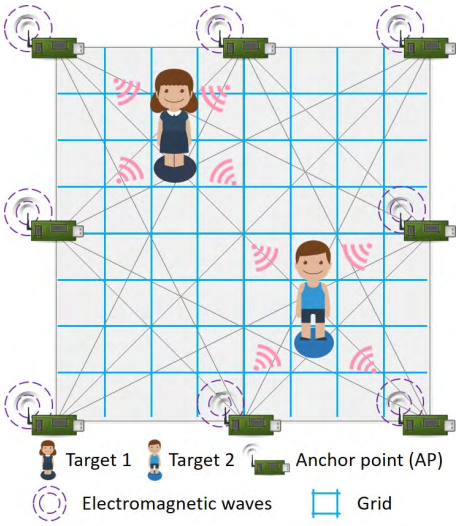

FIGURE 1. Illustration of a device-free localization system.

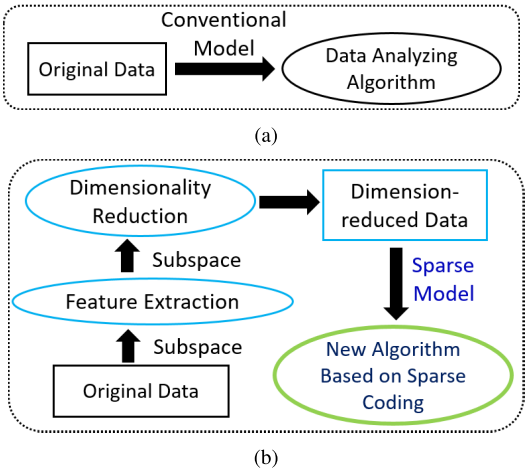

FIGURE 2. Schematic graph for procedures of the conventional approach and proposed DFL approach based on sparse coding in subspace. (a) Routine of the conventional approach. (b) Routine of the proposed approach.

receiving wireless signals in other APs collaboratively. These transmitting-receiving correspondences are different for the case without any targets and the case with some targets, as well as the case that targets appear at different locations. Therefore, the targets can be detected and the locations can be estimated by the tiny RF signal variations induced by the targets. Based on this principle, many methods are proposed for target localization.

However, since the limitation of their algorithms, many methods are just applicable for locating the single target and not applicable for locating multi-targets, which will be limited in the practical DFL applications. In addition, it is easy of imaging that the accuracies of detection and localization are closely dependent on the number of APs. To achieve a fine localization accuracy and to enlarge the monitoring area, most of DFL approaches need to deploy a sufficient number of nodes and collect large amounts of received signal strength (RSS) measurements. However, especially in the emergency scenarios, the accurate information of the targets' locations needs to be acquired as soon as possible; it is crucial to reduce the total localization time of DFL without much sacrificing the accuracy. Whereas, according to Wilson's RF-based model [15], the total number of links increases quadratically as the number of nodes in the network increases, which will result in a problem in practical DFL application due to the high dimensional data. This heavily burdens the processing of DFL.

Basically, according to the framework of Fig. 2(a), many conventional data analyzing algorithms of DFL are essentially based on the methods of deep learning based on autoencoder (DL-AE) [16], K-nearest-neighbor (KNN) [17], orthogonal matching pursuit (OMP) [18], basis pursuit (BP) via linear programming (BP-LP) [19], genetic algorithm (GA) [20], and so on. However, when faced the problem of high-dimensional data, OMP as a greedy algorithm may not provide the accurate enough estimations of locations [21]. And the linear programming based BP and genetic manipulation are highly inefficient [22], [23].

For solving the above problems, in this paper, we propose an accurate and efficient DFL approach which is not only applicable for locating single target, but also multi-targets. The basic structure of the proposed approach has been shown in Fig. 2(b), in which we have also paralleled the conventional one, for a comparison. Before the comparison, for an accessibility of the DFL problem, we need to explain why DFL can be formulated as a sparse-representation-based classification (SRC) problem.

Back to Fig. 1, the monitoring area is discretized into grids, only the target locations are regarded with a non-zero presentation as an obstacle and can attenuate the energy of signal broadcasting. In the testing stage, DFL is based on the configurations of RSS measurements when the target locates at different positions. That is the measurement configurations from some different classes if targets are at variate positions, so that DFL can be regarded as a problem of classification. Due to the sparse nature of target localization that the number of targets' locations is far less than the number of all grids in the monitoring area, the classification can be performed by sparse representation and leading SRC algorithm, which leads it to be a SRC problem.

Hence, inspired by the sparse nature of target localization and the high efficiencies of some sparse-coding algorithms, we formulate DFL with a sparse model expected to achieve a fine accuracy and a high efficiency. Then, we can observe Fig. 2 that the conventional DFL problems mainly incorporate two portions:

a) the acquisition of data from sensors, and b) the DFL execution. Thus, we may accelerate the localization in two considerations: a) reduce dimensions of the original dataset; and/or b) lower the computational complexity of DFL algorithm. Via an extensive review of the existing studies, we find

that the first consideration is mainly focused on achieving dimensionality reduction only in the row-dimensions (Rdims). Moreover, the second consideration has been being widely concerned [11], [24], [25].

Discriminating with the conventional works, in order to achieve a more efficient DFL with higher localization accuracy, we proposed a scheme that can incorporate the two considerations, which will be processed in three corresponding steps. Firstly, it extracts features for each sub-dataset and comprises them into one column, which is achieved dimensionality reduction on the column-dimensions (Cdims). And then, further perform dimensionality reduction on the Rdims. This proposed scheme can reduce the dimensions of DFL data greatly but can keep the main chunk of information in the original data. Finally, we shall find or propose an optimal DFL algorithm to estimate the target location via sparse coding, mainly in the sense of localization accuracy, processing speed, and the data-quantity dependence, based on the sparse model.

It is worth noting that, contrasting to the previous works e.g. [13], [15], [26], in our sparse model, the sensing matrix (e.g. dictionary) $\mathbf{W}$ is constructed by the raw RSS measurements, while its processing is very simple, i.e., just arranging the RSS measurements as the columns of sensing matrix and the column numbers corresponding to the known locations of targets. We do not use the change of RSS measurements to detect the targets and to estimate their locations, rather we use the raw RSS measurements, although finally the classification problem can still be solved by the proposed algorithms.

On the other hand, as in most practical applications, the sensor signal variation induced by a target is tremendous weak; how to obtain DFL estimation with high accuracy remains a challenging problem. Furthermore, the complex noises in the radio band make the weak signal with a very poor signal-to-noise ratio (SNR); and in a dynamic propagating environment, the multi-path effects may induce signal fading so that the signal quality becomes worse. Thus developing an accurate and efficient DFL algorithm that can work under such situations becomes important.

In this paper, in order to address the problems incurred by the requirement of high localization accuracy and high-dimensional data, we regard DFL as a SRC problem, present an accurate and efficient DFL approach which is not only applicable for locating a single target, but also multi-targets. It is essentially different from the conventional compressive-sensing-based localization models, in the sense different designs of observation signal and dictionary, and then proposes two sparse-coding-based approaches to achieve DFL. Particularly, on the one hand, we incorporate a novel convex-optimization-based approach of sparse coding via the iterative shrinkage-thresholding algorithm (SC-ISTA) for target localization. On the other hand, we further propose a subspace-based sparse coding (SSC)-scheme that can achieve dimensionality reduction both in the directions of Rdims and Cdims. Specifically, it firstly conducts the procedure of feature extraction and dimensionality reduction, followed by performing sparse coding in the low-dimensional signal subspace, which leads to the second algorithm termed as subspace-based SC-ISTA (SSC-ISTA). Finally, experiments on real-world dataset are conducted in locating sparsely distributed targets, for evaluating the performances of the proposed algorithms and comparing with three machine-learning algorithms, including DL-AE, KNN, and OMP. To the best of our knowledge, such an SC-ISTA approach and the SSC-scheme for target localization, which aims at achieving a highly accurate and efficient procedure of DFL, have not been well investigated in the literature.

The major contributions of our study can be summarized as follows:

- We present a sparse-representation-based DFL model and propose a sparse coding-based approach for single-target or multi-target localization.
- We propose an SSC-scheme that reduces the dimensions of DFL data greatly but can keep the main chunk of information in the original data, performing sparse coding in the low-dimensional signal subspace.
- The accuracy and efficiency of the proposed approaches and three compared algorithms are validated on the real-world dataset under different levels of noise.

The remainder of this paper is organized as follows. Section II gives an overview of the related works. Section III introduces the system model and problem formulation. The proposed SC-ISTA algorithm and SSC-ISTA algorithm is presented in Section IV. Section V demonstrates the performance evaluation results. Finally, section VI concludes this work.

II. RELATED WORK

DFL is a promising technology that attracts extensive attention; many existing studies have been conducted in the past few years. In this section, a brief literature review of several typically related studies is given below.

A. DEVICE-FREE LOCALIZATION (DFL)

Many DFL approaches have been proposed, including fingerprinting approaches, geometric approach, radio tomographic imaging (RTI) approach, and compressive sensing (CS) approach, etc.

Youssef *et al.* [27] firstly introduced the concept of Device-free Passive localization; and then in their later studies [28], [29], the localization as a fingerprint-matching problem has been formulated for WiFi-based DFL. Zhang *et al.* [30] proposed a typical geometric approach and obtained the dynamic property of a signal that codes the time-dependent RSS behaviors of DFL system. Experiments were conducted with a 4×4 sensor grid covering an area of $12\text{m} \times 9\text{m}$. Then, in their subsequent work [31], the localization model was improved by introducing more sensor nodes to eliminate the noise effects and increase the locating area to $20\text{m} \times 20\text{m}$. Wilson and Patwari [15] formulated the DFL problem as an inverse problem of linear equation system. The linear equation system is usually undetermined

so that its inverse problem is ill-posed. They solved it using a regularization method, and originally achieved the DFL by the RTI technique. According to their formulation, the total number of links might be increased quadratically with the number of nodes. Some works [26], [32], [33] formulated DFL as a problem of sparse signal reconstruction and employed the CS algorithms for reconstruction, i.e., target positions [22], [23]. The fingerprint-based method was also adopted in many other DFL works [34]–[36]; in their views, the localization problem could be formulated as a fingerprint-matching problem. A training database was built by using signal measurements of each link, being gathered as a person moved to predetermined locations in the monitoring area.

The above researches provided a foundation for further DFL studies. However, in order to achieve a fine localization accuracy or expand the localization area, these approaches need to deploy too many nodes, which will result in a large volume of DFL data with high-dimensions. This heavily burdens the processing of DFL and limits the application scope. For solving the problems, in this paper, we formulate the DFL as an SRC problem and utilize the convex-optimization-based sparse coding method and the subspace technique to achieve an accurate and efficient DFL.

B. DFL MODEL AND ALGORITHM

Based on the feature of the target localization and the relationship between the configurations of RSS measurements and the target states, many models were proposed in the past studies.

Wilson and Patwari [15] proposed a linear model for using RSS measurements to image the attenuation caused by objects, and then Xiao *et al.* [37] proposed a nonlinear optimization model for DFL with RTI reconstruction. Guo *et al.* [13] proposed an exponential-Rayleigh model for RSS-based DFL and tracking. Wang *et al.* [26], [32] proposed a CS theory based dynamic statistical model and applied a Bayesian greedy matching pursuit (BGMP) algorithm to locate the target. In this work, the DFL problem was viewed as how to estimate the target location information vector $\Delta\mathbf{p}$ based on the change of the RSS link measurements $\Delta\mathbf{R}$ and the weighting matrix $\mathbf{W}$; in the CS based model $\Delta\mathbf{R}$ was determined by the shadowing loss difference of the two time instants and $\mathbf{W}$ was defined by an ellipse model. Wang *et al.* [19] presented the sparse representation model for DFL and applied a CVX tool that is essentially based on BP-LP algorithm to solve the ℓ_1-norm constrained minimization problem [38]. Whereas, according to [22] and our numerical experiments, BP-LP algorithm was inefficient when faced with the high dimensional data, which cannot meet the requirement of real-time tracking targets. Moreover, [19] only focused on locating the single target, did not investigate the problem of multi-targets localization, which is very important in the practical DFL application. Wang *et al.* [39] achieved frequency-modulation-based DFL and activity recognition via sparse representation. Liu *et al.* [40] also employed the sparse representation model for indoor localization and applied the conventional sparse coding algorithms, LP and OMP, to solve an ℓ_1-norm constrained minimization problem. Different from the other models, such as RTI-based model, etc., we present a sparse-representation-based model of multi-target localization. On the algorithm, distinguishing with the conventional sparse coding algorithms, e.g., BP-LP and OMP etc., we invoke a state-of-the-art algorithm, ISTA, to conduct sparse coding for the efficiency in handling the higher-dimensional data in DFL.

C. SUBSPACE TECHNIQUE IN DFL

The existing studies mentioned above mainly focus on accuracy, none of them mention the problem of efficient computation with dimension-reduction. In a recent research works, Liu *et al.* [24] proposed an approach of redundancy reduction for indoor device-free localization, using principal component analysis (PCA) technique for node reduction. They formulated the node reduction problem as a redundancy control problem and controlled node redundancy using a genetic algorithm. Wang *et al.* [19] utilized the Eigen-Value-Decomposition (EVD) to deal with the problems of outliers and noise. However, since their purpose was for improving the accuracy by feature extraction, not for improving the efficiency via the subspace technique, they did not consider the efficiency of their proposed approach. Therefore, their work led to dimensionality reduction only on the Cdims. Whereas, according to [15], the row-dimensions increases quadratically as the number of nodes in the network increases. This will result in a large volume of DFL data with high Rdims and heavily burden the processing of DFL in the practical application. Zhao and Patwari [41] applied a subspace decomposition method based on PCA technique to noise reduction for variance-based device-free localization and tracking. Experimental results show that their proposed algorithm reduces localization root mean squared error (RMSE) by 41%. Such results are far from the requirement of the most realistic applications; it also means that the subspace could not catch the main chunk of information in the original data.

In the above works, most of them applied the subspace technique for the purposed of denoising or energy-harvesting. All of them considered the dimensionality reduction only on the single direction of the dataset. However, for most of the real-world DFL datasets, both the Rdims and the Cdims are with the high dimensions, and either direction may burden the DFL algorithms. Thus, it will be necessary to investigate the dimensionality reduction both on the row-dimensions for improving the efficiency.

III. PROBLEM STATEMENT

A. PRELIMINARY AND SYSTEM MODEL

As shown in Fig. 3, for a more accessibility of the problem, we discretize the monitoring area of DFL system into grids, only the target locations are regarded with a non-zero

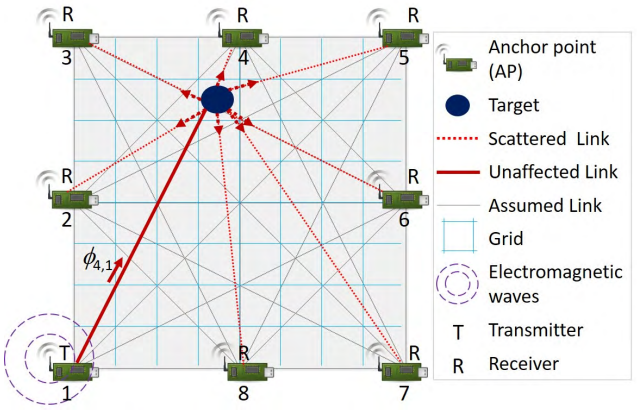

FIGURE 3. Illustration of a device-free localization system model.

presentation as an obstacle and can attenuate the energy of signal broadcasting. That is, a target in the detection area of DFL system will disturb the values of the RSS measurements at APs; and then, different joint signal configurations comprised of RSS measurements will be obtained when the target is at different positions.

In the testing stage, DFL is based on the configurations of RSS measurements when the target locates at different positions. That is the measurement configurations from some different classes if a target is at variate positions, so that DFL can be regarded as a problem of classification. There exists many methods being proposed for solving the problems of classification or cluster [42]–[44], e.g. [44] utilized the deep learning models to address the problem of image classification. Whereas, due to the sparse nature of target localization, that the number of target locations is far less than the number of all grids in the monitoring area, the classification problem can be well performed by sparse representation and leading SRC algorithm.

In the DFL system, a wireless sensor node is normally termed as the anchor point (AP) [45]. As shown in Fig. 3, all the APs are transmitter-receivers that are fixed to surround the monitoring area and communicate with each other. These APs work as a transmitter in turn, according to a schedule; in other words, only one AP transmits signal at each time and other APs receive signals. For an easy explaining, we take the first AP transmitting signals as an example in Fig. 3. When a target moves into the monitoring area, it may absorb and scatter some of the transmitted signals. And then RSS measurements of the affected links will be changed, which makes it possible to realize DFL based on the configurations of RSS measurements.

In DFL applications, in order to improve the locating accuracy and broaden the monitoring area, the number of APs and RPs will accordingly increase, which will result in the scales of the dataset being increased drastically, and then burden the computation of DFL algorithm. Therefore, the DFL will be very slow when faced with the larger scale of the dataset. In order to accelerate the localization without much sacrificing the accuracy, in this paper, a subspace-based scheme that can reduce the dimensions of the original dataset is proposed to lower the computing burden, and then an optimally sparse-coding-based DFL algorithm is utilized to maintain the accuracy.

Subspace technique based on eigenvalue decomposition is a classical feature extraction and data representation technique which is widely used in the areas of image compression, pattern recognition, and computer vision. One of the main advantages of subspace technique is that, through subspace transform, the signal components are completely uncorrelated, and the energy contained in the signal is maximally concentrated in a small number of components. Then, the data can be compressed by reducing the number of dimensions, without much loss of information. Hence, in this paper, the subspace technique is used to reduce dimensions of original DFL data, and the procedure of implementing the subspace technique is given in detail in later subsection IV-B. The detailed steps of implementing the sparse-coding-based algorithm are given in items 4) and 5) of subsection III-B. The major notations used in this paper are summarized in Table 1.

B. PROBLEM FORMULATION

Suppose that the node number of monitoring area is L. As shown in Fig. 3, each of APs works as a transmitter in turn from the 1-st AP to the 8-th AP. Let $\phi_{i,j}$ denotes the RSS measurement received at the i-th node which is transmitted by the j-th node while an object is at a known position, for example, $\phi_{4,1}$ in Fig. 3. And then the vector $\boldsymbol{\phi}_i$ consists of RSS measurements at the i-th node from all L nodes, which is defined as

$$\boldsymbol{\phi}_i = [\phi_{i,1},\ \phi_{i,2},\ \cdots,\ \phi_{i,L}]^T \in \mathbf{R}^L \tag{1}$$

where $\bullet^T$ is the transpose.

As it is impossible for each node to receive RSS transmitted by itself, we fix $\phi_{i,i}$ a constant value to each node, being equivalent to the received RSS measurement from itself. Then, when DFL system is working, an RSS matrix $\boldsymbol{\Phi}$ contained all the links can be obtained

$$\begin{aligned}\boldsymbol{\Phi} &= [\boldsymbol{\phi}_1,\ \boldsymbol{\phi}_2, \cdots, \boldsymbol{\phi}_L]^T \\ &= \begin{bmatrix} \phi_{1,1} & \phi_{1,2} & \cdots & \phi_{1,L} \\ \phi_{2,1} & \phi_{2,2} & \cdots & \phi_{2,L} \\ \vdots & \vdots & \ddots & \vdots \\ \phi_{L,1} & \phi_{L,2} & \cdots & \phi_{L,L} \end{bmatrix} \in \mathbf{R}^{L\times L}\end{aligned} \tag{2}$$

Therefore, there will be $m = L \times L$ elements in an RSS matrix $\boldsymbol{\Phi}$. In our DFL system, two stages or modes, i.e., the constructing dictionary stage and the unknown target detection-localizing stage, are involved. The details are given in the following subsections.

1) THE CONSTRUCTING DICTIONARY STAGE

As shown in Fig. 4, the monitoring area is discretized into K grids. If we predefine a reference point (RP) at each grid,

TABLE 1. Symbols and variables.

Notations	Description
$\phi_{i,j}$	RSS measurement that is shown in Fig. 3
ϕ_i	a vector, consisting of RSS measurements transmitted from all the L nodes to the i-th node, is defined in (1)
$\mathbf{\Phi}$	RSS matrix that is defined in (2)
$\mathbf{w}_{qb}$	sample vector that is defined in (3).
$\mathbf{W}_q$	sample matrix that is associated with the q-th RP and defined in (4)
$\mathbf{W}$	dictionary which is defined in (5) and shown in Fig. 6.
$\mathbf{y}$	observation vector that is defined in (6).
α_{pj}	coefficient of $\mathbf{w}_{pj}$ which is shown in (7).
α	sparse coefficient vector that is shown in (8)
$\alpha^\star$	sparse solution of problem (9), (10), (12) and (13)
α^*	sparse vector which is transformed from $\alpha^\star$, according to $\alpha_p^*=\Sigma_{j=1}^{\tau}\alpha_{pj}^\star$, (16) and (17).
$\|\cdot\|_0$	ℓ_0-norm that counts the number of nonzero elements in a vector.
$\|\cdot\|_1$	ℓ_1-norm that is defined as $\|\mathbf{x}\|_1=\sum_i x_i$.
$\|\cdot\|_2^2$	ℓ_2-norm which is defined as $\|\mathbf{x}\|_2^2=\sum_i(x_i)^2$
μ and ρ	scaling parameters that are used to trade off the two terms in problem (13) and (29), respectively
h_θ	shrinkage operator that is defined in (15)
φ	index of a specific element in sparse vector α^* or $\beta^\star$, as well as the ID number of estimated testing location, which is defined in (18) or (31)
$\mathbf{U}$	semi-transformation matrix that is defined in (22)
$\mathbf{S}_k$	transforming matrix associated with the specific subspace which is defined in (25)
λ	eigenvalue that is shown in Table 2
k	row-dimensions of the dimension-reduced data
$\mathbf{W}_{appr}$	new approximate dictionary in a subspace which is defined in (27)
$\mathbf{y}_{appr}$	new observation vector that is defined in (28)
$\beta^\star$	sparse solution of problem (29)
Rdims; Cdims	row-dimensions; column-dimensions
RoC	ratio of cumulative distribution that is defined in (26)
ISTA	iterative shrinkage-thresholding algorithm
SC-ISTA	sparse coding via iterative shrinkage-thresholding algorithm
SSC-ISTA	subspace-based sparse coding via iterative shrinkage-thresholding algorithm
DL-AE	deep learning approach based on autoencoder
KNN	K-nearest-neighbor
OMP	orthogonal matching pursuit

the K RPs can be regarded as K classes based on their positions, that is, positions within a grid is in one class.

For the first step, an object that is viewed as an assumed-target, e.g. a person, is put at one of the RPs. Meanwhile, each of APs transmits signal by turns according to a schedule and the other RPs receive the RSSs which are organized as RSS matrix as (2). And then, we conduct the first step for several times, i.e., trials, at each RP. Since the object can be put inside the different grids, we repeat the above steps for all K RPs, and the wireless propagation can vary from time to time. Without loss of generality, we take the q-th RP as an example. Specifically, we put an object at the q-th RP and conduct τ trials, and then we can get τ RSS matrices

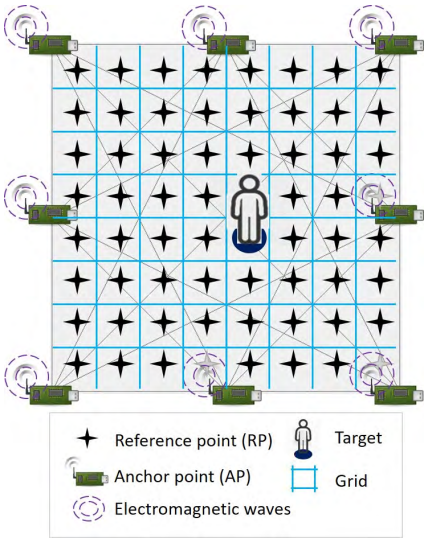

FIGURE 4. Illustration of constructing dictionary stage and testing stage.

$\{\mathbf{\Phi}_{q1}, \mathbf{\Phi}_{q2}, \cdots, \mathbf{\Phi}_{qb}, \cdots, \mathbf{\Phi}_{q\tau}\}$. Here $\mathbf{\Phi}_{qb}(1 \le b \le \tau)$ is the b-th RSS matrix measured at the q-th RP, as defined in (2). By doing vectorization on each RSS matrix as

$$\mathbf{w}_{qb} = vec(\mathbf{\Phi}_{qb})\ (1 \le b \le \tau) \tag{3}$$

where $\mathbf{w}_{qb} \in \mathbf{R}^m$ is the b-th sample vector of the q-th RP. Then we arrange the τ sample vectors of the q-th RP as columns of a matrix $\mathbf{W}_q$, which is constructed as follows

$$\mathbf{W}_q = [\mathbf{w}_{q1}, \mathbf{w}_{q2}, \cdots, \mathbf{w}_{qb}, \cdots, \mathbf{w}_{q\tau}] \in \mathbf{R}^{m\times\tau}, \quad (1 \le q \le K) \tag{4}$$

where $m = L \times L$, $\mathbf{W}_q$ is the sample matrix of the q-th RP, and $\mathbf{w}_{qb}$ is the b-th column of $\mathbf{W}_q$.

If we respectively conduct τ trials at each of the total K RPs, there will be K sample matrices that each of them is similar to $\mathbf{W}_q$. And then, by arranging the $n = K \times \tau$ sample vectors together, we form a new matrix $\mathbf{W}$ which contains n sample vectors. Thus, $\mathbf{W}$ consisting of all samples is organized as a dictionary, or say, the sensing matrix, which is with position labels that are corresponding to the subscript of $\mathbf{W}_q$. Then $\mathbf{W}$ is constructed as follows:

$$\begin{aligned}\mathbf{W} &= [\mathbf{W}_1, \mathbf{W}_2, \cdots, \mathbf{W}_q, \cdots \mathbf{W}_K] \\ &= [\mathbf{w}_{11}, \mathbf{w}_{12}, \cdots, \mathbf{w}_{K\tau}] \in \mathbf{R}^{m\times n}\end{aligned} \tag{5}$$

where $\mathbf{W}$ is termed as the **dictionary**.

2) THE TESTING STAGE AND THE LINEAR COMBINATION OF A TESTING SIGNAL

In this stage, as shown in Fig. 4, when a testing target is put into the DFL area, a (testing) observation signal $\mathbf{y}$ will be obtained as

$$\mathbf{y} = vec(\mathbf{\Phi}) \tag{6}$$

where $\mathbf{y} \in \mathbf{R}^m$ is termed as **observation vector**.

Here, we assume the target is, approximately, at the p-th RP, meaning that target belongs to the p-th class. If sufficient samples of the p-th RP are given, i.e. conducting enough trials at the p-th RP in the stage of constructing dictionary, the new testing sample $\mathbf{y}$ of the target near to the p-th RP can be approximately represented with the p-th sample matrix $\mathbf{W}_p$, given as follows:

$$\begin{aligned}\mathbf{y} &= \mathbf{W}_p\boldsymbol{\alpha}_p \\ &= \Sigma_{l=1}^{\tau}\mathbf{w}_{pl}\alpha_{pl} \\ &= \alpha_{p1}\mathbf{w}_{p1} + \alpha_{p2}\mathbf{w}_{p2} + \cdots + \alpha_{pn}\mathbf{w}_{p\tau},\ (1 \le p \le K) \end{aligned} \quad (7)$$

where $\boldsymbol{\alpha}_p = [\alpha_{p1}, \alpha_{p2}, \cdots, \alpha_{p\tau}]^T \in \mathbf{R}^{\tau}$ is a vector comprised of coefficients, $\alpha_{pj} \in R$ is the coefficient of each term.

3) SPARSE MODEL AND THE SPARSE REPRESENTATION OF A TESTING SIGNAL

Consider the samples in Fig. 5 as an example, where the dataset consists of 90 points from nine classes. The red square shows the test signal and the others are training samples of the dictionary. It can be seen that, if test signal belongs to the 1-st class, the selected samples that are marked in blue triangles with nonzero coefficients of SRC for representing the red square mainly involves the ones from the 1-st class.

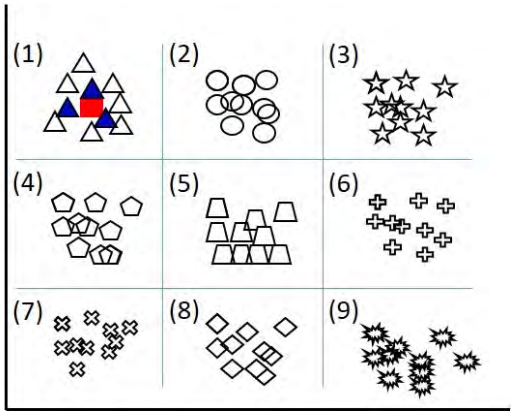

FIGURE 5. Illustration for sparse-representation-based classification (SRC) of a testing signal.

Based on the above view and the result of item 2) of subsection III-B, the linear representation of observation vector $\mathbf{y}$ can be sparsely represented in terms of n sample vectors of the dictionary as

$$\mathbf{y} = \mathbf{W}_p\boldsymbol{\alpha}_p = \mathbf{W}\boldsymbol{\alpha} \quad (8)$$

where $\boldsymbol{\alpha} = [0, \cdots, \alpha_{p1}, \alpha_{p2}, \cdots, \alpha_{p\tau}, \cdots, 0]^T \in \mathbf{R}^n$. (8) becomes a sparse representation problem, since $\boldsymbol{\alpha}$ is corresponding a sparse coefficient vector of which nonzero elements are associated to the location of the target.

Based on the above description, when the target is close to a certain RP, the observation signal in the testing stage can be sparsely represented by a few basis signals of that RP. Therefore, DFL is essentially an SRC problem, that is, SRC [46] aims to reconstruct an input (testing) signal using a small set of elements parsimoniously chosen from the over-complete dictionary, and classifies the testing signal into the class which results in the minimal reconstruction error. Hence, the DFL problem can be effectively solved by the sparse coding method in the field of sparse representation. For an easy understanding, we present the entire model in Fig. 6. It is worthy of note that one target may have several corresponding components in $\boldsymbol{\alpha}$.

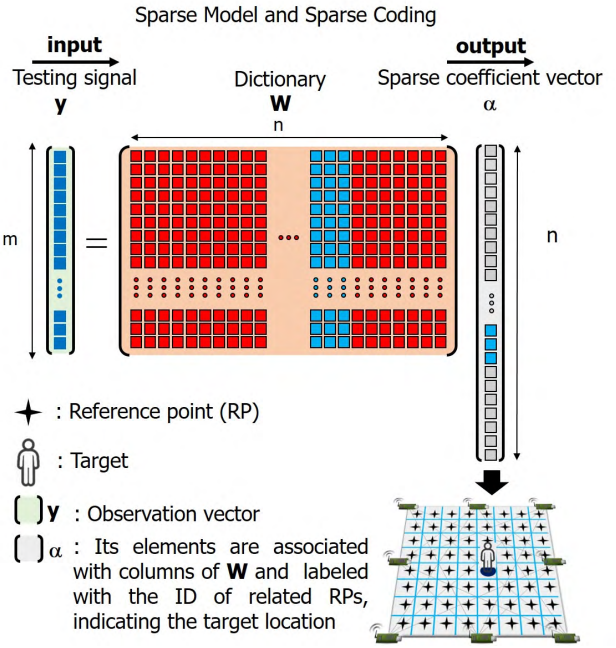

FIGURE 6. Illustration of the sparse model and the procedure of sparse coding for target localization.

4) SPARSE CODING

Sparse coding is the process of computing the coefficient vector based on the set of observation signals $\mathbf{y}$ and a known dictionary $\mathbf{W}$, as shown in Fig. 6. Based on the formulation described in the item 3) of subsection III-B, if we can obtain the sparse solutions by solving (8) via sparse coding, then the target location can be known.

For $\mathbf{W} \in \mathbf{R}^{m\times n}$, it is obvious that, if $m > n$, (8) is an overdetermined system, and the unique solution can usually found. However, in most cases of DFL application, we face the case that $m < n$, because, in the constructing dictionary stage of constructing dictionary, the larger the number of trials τ conducted on each RP is, the better locating accuracy will be, which will make it possible that the total number of columns $n = K \times \tau$ is larger than m.

However, if $m < n$ which means that (8) is an undetermined system, its solution is not unique, i.e., the problem is ill-posed. By selecting the sparsest solution, we can make the problem well-posed. Since the direct sparsity measure is through ℓ_0-norm which is a measure of the number of nonzero elements in a vector, this motivates us to solve the following optimization problem of ℓ_0-norm to find the sparsest solution

of (8):

$$\boldsymbol{\alpha}^{\star} = \underset{\boldsymbol{\alpha}}{argmin}\|\boldsymbol{\alpha}\|_0 \quad subject\ to\ \mathbf{y} = \mathbf{W}\boldsymbol{\alpha} \tag{9}$$

where ℓ_0-norm $\|\boldsymbol{\alpha}\|_0$ counts the number of nonzero elements in $\boldsymbol{\alpha}$.

Unfortunately, the problem (9) of finding the sparsest solution of linear equation in an undetermined system has been proven to be NP-hard, because it is required to enumerate subsets of the dictionary looking for the smallest subset able to represent the signal, which results in the complexity grows exponentially with the number of columns of dictionary. Moreover, the ℓ_0-norm is non-differentiable and non-convex, therefore some greedy algorithms, including matching pursuit and OMP, are proposed to solve the problem (9), suboptimally. However, greedy algorithms are not efficient when facing high-dimensional DFL data.

According to [47] and [48], highly sparse solutions can be obtained by convex optimization with ℓ_1-norm. Hence, we consider replacing the ℓ_0-norm in (9) by the following ℓ_1-norm minimization problem

$$\boldsymbol{\alpha}^{\star} = \underset{\boldsymbol{\alpha}}{argmin}\|\boldsymbol{\alpha}\|_1 \quad subject\ to\ \mathbf{y} = \mathbf{W}\boldsymbol{\alpha} \tag{10}$$

Since real data are noisy, the model (8) can be modified to account for possibly dense noise as

$$\mathbf{y} = \mathbf{W}\boldsymbol{\alpha} + \boldsymbol{\nu} \tag{11}$$

where $\boldsymbol{\nu} \in \mathbf{R}^m$ is a noise term with a boundary of $\|\boldsymbol{\nu}\|_2^2 < \epsilon$, and when $\boldsymbol{\nu} = \mathbf{0}$, it is the noiseless case. Then, considering the noise, (10) is modified as

$$\boldsymbol{\alpha}^{\star} = \underset{\boldsymbol{\alpha}}{argmin}\|\boldsymbol{\alpha}\|_1 \ \ subject\ to\ \|\mathbf{y} - \mathbf{W}\boldsymbol{\alpha}\|_2^2 < \epsilon \tag{12}$$

For sparse coding, a more popular modified form of (12) is using ℓ_1 regularization method, in which one seeks to find a solution of

$$\boldsymbol{\alpha}^{\star} = \underset{\boldsymbol{\alpha}}{argmin}\frac{1}{2}\ \|\mathbf{y} - \mathbf{W}\boldsymbol{\alpha}\|_2^2 + \mu\|\boldsymbol{\alpha}\|_1 \tag{13}$$

where the first term with the square of ℓ_2-norm is a measure of distance between observation signal and estimated signal, and the second term with ℓ_1-norm is a measure of sparsity which associated with the range of possible locations of the target. μ is a small empirical constant, termed as scaling constant, which trades off the first term of error and the second term of sparsity.

5) ITERATIVE SHRINKAGE-THRESHOLDING ALGORITHM (ISTA)

In this paper, we use the iterative shrinkage-thresholding algorithm [49] to optimize the object function (13). For a clear summarization, we present the method in the block diagram of Fig. 7. Specifically, we perform sparse coding by the following main steps

$$\begin{aligned} \boldsymbol{\alpha}_{k+1} &= h_\theta\left(\frac{1}{C}\mathbf{W}^T\mathbf{y} + \left(\mathbf{I} - \frac{1}{C}\mathbf{W}^T\mathbf{W}\right)\boldsymbol{\alpha}_k\right) \\ \theta &= \frac{\mu}{C},\ \boldsymbol{\alpha}_0 = \mathbf{0} \end{aligned} \tag{14}$$

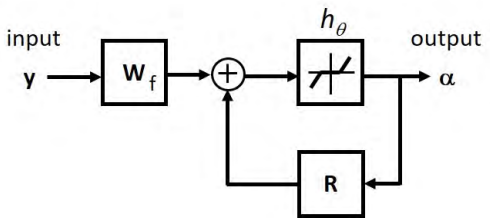

FIGURE 7. Block diagram of the ISTA algorithm for sparse coding, where y is the input, $\mathbf{W}_f = \frac{1}{C}\mathbf{W}^T$, h_θ is the shrinkage function with threshold θ, and $\mathbf{R}=\mathbf{I} - \frac{1}{C}\mathbf{W}^T\mathbf{W}$.

where C is a constant that must be greater than the largest eigenvalue of $\mathbf{W}^T\mathbf{W}$, μ is the scaling constant of (13), $\mathbf{I}$ is an identity matrix, and θ is a threshold which can be calculated according to C and μ. In addition, h_θ is the shrinkage operator defined by

$$h_\theta(x_i) = (|x_i| - \theta)_+ sign(x_i), \quad for\ i = 1, \cdots, n \tag{15}$$

where $(\cdot)_+$ means the operation that returns the positive part.

IV. PROPOSED ALGORITHMS

A. CLASSIFICATION FOR DFL BASED ON THE SPARSE SOLUTION OF SC-ISTA

Through (14) and (15), the solution $\boldsymbol{\alpha}^{\star}$ of the problem (13) can be obtained,

$$\begin{aligned} \boldsymbol{\alpha}^{\star} &= \{\alpha_1^{\star}, \cdots, \alpha_n^{\star}\} \\ &= \{\alpha_{11}^{\star}, \cdots, \alpha_{pj}^{\star}, \cdots, \alpha_{K\tau}^{\star}\}, \\ &\quad for\ p = 1, \cdots, K; \quad j = 1, \cdots, \tau \end{aligned} \tag{16}$$

Based on (16), let $\alpha_p^* = \Sigma_{j=1}^{\tau}\alpha_{pj}^{\star}$, and then $\boldsymbol{\alpha}^{\star}$ is transformed to $\boldsymbol{\alpha}^*$, which is given by

$$\boldsymbol{\alpha}^* = \{\alpha_1^*, \cdots, \alpha_p^*, \cdots, \alpha_K^*\}, \quad for\ \boldsymbol{\alpha}^* \in \mathbf{R}^{K\times 1} \tag{17}$$

If the solution includes only one non-zero component, the corresponding RP position can be taken as the location of the target. If the solution includes several non-zero components:

- For locating a single target, based on (16), the target's location is estimated at the φ-th RP, where φ is given by

$$\varphi = \underset{p}{argmax}\{\alpha_1^*, \cdots, \alpha_p^*, \cdots, \alpha_K^*\} \tag{18}$$

- For locating sparsely distributed N targets, if the N targets' locations are estimated at the φ_1-th RP, ..., φ_N-th RP, where $\varphi_1, \ldots, \varphi_N$ are the subscripts of the elements with decreasing order in vector $\boldsymbol{\alpha}^*$. Based on (17), they are given by

$$\begin{cases} \varphi_1 = \underset{p}{argmax}\{\alpha_1^*, \cdots, \alpha_p^*, \cdots, \alpha_K^*\} \\ \qquad\vdots \\ \varphi_N = \underset{q}{argmax}\{\alpha_1^*, \cdots, \alpha_p^*, \cdots, \alpha_K^*\},\ for \\ \{\alpha_{\varphi_1}^*, \ldots, \alpha_{\varphi_{N-1}}^*\} \not\subset \{\alpha_1^*, \cdots, \alpha_p^*, \cdots, \alpha_K^*\} \end{cases} \tag{19}$$

As the sparse coding algorithm is based on ISTA, the proposed localization algorithm is named as sparse coding via the iterative shrinkage-thresholding algorithm (SC-ISTA), whose pseudo-code is described in Algorithm 1.

Algorithm 1 SC-ISTA

Require: $\mathbf{y} \in \mathbf{R}^m$, $\mathbf{W} \in \mathbf{R}^{m\times n}$, μ, choose C >largest eigenvalue of $\mathbf{W}^T\mathbf{W}$, $\theta = \frac{\mu}{C}$, $\boldsymbol{\alpha}_0 = \mathbf{0}$, $\mathbf{I} = \mathbf{1}$
Ensure: φ or $\{\varphi_1, \ldots, \varphi_N\}$
1: **for** $i = 0$ *to maxiteration* **do**
2: $\quad\boldsymbol{\alpha}_{i+1} \leftarrow h_\theta(\frac{1}{C}\mathbf{W}^T\mathbf{y} + (\mathbf{I} - \frac{1}{C}\mathbf{W}^T\mathbf{W})\boldsymbol{\alpha}_i)$
3: $\quad$Until $\|\boldsymbol{\alpha}_{i+1} - \boldsymbol{\alpha}_i\|_2^2$ below a threshold
4: **end for**
5: $\boldsymbol{\alpha}^\star \leftarrow \boldsymbol{\alpha}_{i+1}$
6: $\boldsymbol{\alpha}^\star$ is transformed to $\boldsymbol{\alpha}^*$ by (17)
7: **if** locate single target **then**
8: $\quad$Determine φ as the ID of target's location by (18)
9: $\quad$**Return** φ
10: **end if**
11: **if** locate sparse N multi-targets **then**
12: $\quad$Determine $\varphi_1, \ldots, \varphi_N$ by (17) and (19)
13: $\quad$**Return** $\{\varphi_1, \ldots, \varphi_N\}$
14: **end if**

B. SSC-SCHEME AND SSC-ISTA FOR DFL

Our preliminary experimental results showed that the current DFL algorithms, including OMP, BP-LP and our proposed SC-ISTA algorithm, will become computation-consuming when the scale of the dataset is larger and larger, and become so large that they are not applicable in most of the practical scenarios. To tackle this problem, in this section, we propose an SSC-scheme which is based on the subspace techniques to do dimensionality reduction both in the directions of Rdims and Cdims for the DFL dataset, and then conduct the SC-ISTA in a low-dimensional subspace to improve the efficiency without sacrificing the localization accuracy.

This is inspired by the subspace techniques used in dimensionality reduction [50] and denoising [51]. We are going to construct a new dictionary in the principal component subspace of signal. Specifically, the whole procedure of SSC-scheme is divided into two main steps which are shown as follows:

1) TRANSFORMATION IN THE DIRECTION OF COLUMN-DIMENSION

From (5), it can be known that the original dictionary $\mathbf{W} = [\mathbf{W}_1, \cdots, \mathbf{W}_q, \cdots, \mathbf{W}_K]$. By conducting the process of zero-mean-normalization on $\mathbf{W}$, subtracting the sample mean and dividing the standard deviation, a corresponding matrix $\mathbf{W}_{norm} = [\mathbf{W}'_1, \cdots, \mathbf{W}'_q, \cdots, \mathbf{W}'_K]$ is obtained. And then, for each RP (i.e., each class), taking the q-th RP as an example, $\mathbf{W}'_q = [\mathbf{w}'_{q1}, \cdots, \mathbf{w}'_{q\tau}]$, its correlation matrix is calculated as follows,

$$\mathbf{M}_q = \frac{1}{\tau}\sum_i^\tau \mathbf{w}'_{qi}\mathbf{w}'^H_{qi}, \tag{20}$$

where $[\cdot]^H$ is conjugate transpose and $\mathbf{M}_q \in \mathbf{R}^{m\times m}$. Then, by Singular-Value-Decomposition (SVD),

$$\mathbf{M}_q = \mathbf{U}_q\boldsymbol{\Sigma}_q\mathbf{V}_q \tag{21}$$

where $\mathbf{U}_q = \{\mathbf{u}_{q1}, \mathbf{u}_{q2}, \ldots, \mathbf{u}_{qm}\}$ is the normalized eigenvector matrix with the size of $m \times m$, where these eigenvectors represent the characteristics of the original dataset, and $\boldsymbol{\Sigma} = diag\{\sigma_1, \sigma_2, \ldots, \sigma_m\}$ is the diagonal singularvalue matrix with all singularvalues sorted in descending order. $\mathbf{u}_{q1}$ is associated with the largest singularvalue σ_1, which represents the most main characteristic of $\mathbf{W}_q$. Thus, after conducting the SVD on all of the total K sample matrices, a semi-transformation matrix $\mathbf{U}$ is obtained as

$$\mathbf{U} = \{\mathbf{u}_{11}, \mathbf{u}_{21}, \ldots, \mathbf{u}_{q1}, \ldots, \mathbf{u}_{K1}\} \tag{22}$$

where $\mathbf{U}$ consists of the eigenvectors associated with the largest eigenvalues of all RPs.

2) DIMENSIONALITY REDUCTION IN THE DIRECTION OF ROW-DIMENSION

Before dimensionality reduction in the direction of row-dimension, it also conducts the process of zero-mean-normalization on $\mathbf{U}$ like the first step, and a corresponding matrix $\mathbf{U}_{norm}$ is obtained. Then, the covariance matrix $\boldsymbol{\Omega}$ of $\mathbf{U}_{norm}$ is calculated as

$$\boldsymbol{\Omega} = \frac{1}{K}\mathbf{U}_{norm}\mathbf{U}^H_{norm} \tag{23}$$

Then we can find the eigenvalues and eigenvectors of $\boldsymbol{\Omega}$ via eigenvalue decomposition (EVD), which is given by

$$\boldsymbol{\Omega} = \mathbf{S}\Lambda\mathbf{S}^T \tag{24}$$

where $\mathbf{S} = \{\mathbf{s}_1, \mathbf{s}_2, \ldots, \mathbf{s}_k, \ldots, \mathbf{s}_m\}$ is the normalized eigenvector matrix with the size of $m \times m$, where these eigenvectors, $\mathbf{s}_1, \ldots, \mathbf{s}_m$, represent the characteristics of the original dataset, and $\boldsymbol{\Lambda} = diag\{\lambda_1, \lambda_2, \ldots, \lambda_m\}$ is the diagonal eigenvalue matrix with $\lambda_1 \geq \lambda_2 \geq \ldots \geq \lambda_m$ sorted in descending order. The terms $\{\mathbf{s}_1, \ldots, \mathbf{s}_k, \ldots, \mathbf{s}_m\}$ and $\{\lambda_1, \ldots, \lambda_k, \ldots, \lambda_m\}$ are the eigenvectors and eigenvalues of $\boldsymbol{\Omega}$, and $\mathbf{s}_k$ is associated with λ_k. The following step is to find the principal component subspace by using a transforming matrix $\mathbf{S}_k$.

$$\mathbf{S}_k = \{\mathbf{s}_1, \mathbf{s}_2, \ldots, \mathbf{s}_k\}, (1 \leq k \leq m), \tag{25}$$

where $\mathbf{S}_k$ is the submatrix of $\mathbf{S}$, and then, we are going to choose k to find $\mathbf{S}_k$. Since the eigenvalues represent the distribution of the source data's energy [52], the cumulative energy content (CEC) for the k-th eigenvector is the sum of

TABLE 2. Sample table for illustrating to choose the minimum dimension (i.e. k) in algorithm SSC-ISTA.

Component	λ_i (eigenvalue)	CEC (cumulated eigenvalue)	RoC (cumulated percentage)
1	λ_1	λ_1	$\frac{\lambda_1}{\sum_{j=1}^{m}\lambda_j}$
2	λ_2	$(\lambda_1+\lambda_2)$	$\frac{\lambda_1+\lambda_2}{\sum_{j=1}^{m}\lambda_j}$
⋮	⋮	⋮	⋮
k	λ_k	$\sum_{z=1}^{k}\lambda_z$	$\frac{\sum_{z=1}^{k}\lambda_z}{\sum_{z'=1}^{m}\lambda_{z'}}$ (threshold)
⋮	⋮	⋮	⋮
m	λ_m	$\sum_{z=1}^{m}\lambda_z$	100%

the energy content across all of the eigenvalues from 1 to k. Then k can be determined by

$$RoC = \frac{CEC\ of\ the\ important\ components}{CEC\ of\ all\ components} = \frac{\sum_{z=1}^{k}\lambda_z}{\sum_{z=1}^{m}\lambda_z}, (1 \le k \le m), \quad (26)$$

where RoC is short for the ratio of cumulative distribution which is used as a criterion to choose k.

Hence, the goal is to choose a value of k as small as possible while achieving a reasonably high value of RoC on a percentage basis. In order to make the procedure easy to understand, we make the sample Table 2 to help illustrate the following steps. For example, one may want to choose k so that the RoC is above a certain threshold γ, like 97%. In this case, γ is set to be 97% and choose the smallest value of k, and then the transforming matrix $\mathbf{S}_k \in \mathbf{R}^{m\times k}$ can be found based on (25) and (26). As a result, $\mathbf{S}_k$ is consist of the eigenvectors associated with principal components, which spans the signal principal component subspace.

Therefore, in the constructing dictionary stage, a new approximate sample dictionary $\mathbf{W}_{appr}$, which is transformed to the signal principal component subspace via $\mathbf{S}_k$, can be obtained by

$$\mathbf{W}_{appr} = \mathbf{S}_k^T\mathbf{U} \quad (27)$$

where $\mathbf{S}_k^T \in \mathbf{R}^{k\times m}$ is the transpose of $\mathbf{S}_k$ and $\mathbf{W}_{appr} \in \mathbf{R}^{k\times K}$ is the new dictionary after reducing dimension on the original dictionary $\mathbf{W}$.

In the testing stage, when a testing target is put into the DFL area, the new approximate observation vector $\mathbf{y}_{appr}$ can be obtained from (28)

$$\mathbf{y}_{appr} = \mathbf{S}_k^T\mathbf{y} \quad (28)$$

where $\mathbf{y}_{appr} \in \mathbf{R}^{k\times 1}$ is the new observation after reducing dimension for original observation signal $\mathbf{y}$.

Hence, similar to the procedure of SC-ISTA, the target can be located by solving the following problem:

$$\boldsymbol{\beta}^\star = \underset{\boldsymbol{\beta}}{argmin}\frac{1}{2}\|\mathbf{y}_{appr} - \mathbf{W}_{appr}\boldsymbol{\beta}\|_2^2 + \rho\|\boldsymbol{\beta}\|_1 \quad (29)$$

where $\boldsymbol{\beta}$ is the coefficient vector, $\boldsymbol{\beta}^\star$ is the sparse solution. Then, through (14) and (15), $\boldsymbol{\beta}^\star$ can be obtained as,

$$\boldsymbol{\beta}^\star = \{\beta_1^\star, \cdots, \beta_p^\star, \cdots, \beta_K^\star\} \quad for\ p = 1, \cdots, K;\ \boldsymbol{\beta}^\star \in \mathbf{R}^{K\times 1} \quad (30)$$

If the $\boldsymbol{\beta}^\star$ includes only one non-zero component, the corresponding RP position can be taken as the location of the target. If the solution includes several non-zero components:

- For locating a single target, based on (30), the target's location is estimated at the φ-th RP, where φ is given by

$$\varphi = \underset{p}{argmax}\{\beta_1^\star, \cdots, \beta_p^\star, \cdots, \beta_K^\star\} \quad (31)$$

- For locating sparsely distributed N targets, the N targets' locations are estimated at the φ_1-th RP, ..., φ_N-th RP, where $\varphi_1, \ldots, \varphi_N$ are the subscripts of the elements with decreasing order in vector $\boldsymbol{\beta}^\star$. Based on (30), they are given by

$$\begin{cases} \varphi_1 = \underset{p}{argmax}\{\beta_1^\star, \cdots, \beta_p^\star, \cdots, \beta_K^\star\} \\ \quad\vdots \\ \varphi_N = \underset{p}{argmax}\{\beta_1^\star, \cdots, \beta_p^\star, \cdots, \beta_K^\star\},\ for \\ \{\beta_{\varphi_1}^\star, \ldots, \beta_{\varphi_{N-1}}^\star\} \not\subset \{\beta_1^\star, \cdots, \beta_p^\star, \cdots, \beta_K^\star\} \end{cases} \quad (32)$$

As $\mathbf{W}_{appr}$ and $\mathbf{y}_{appr}$ are constructed in principal component subspace, and then solve the problem with SC-ISTA. Thus, the proposed algorithm is termed as SSC-ISTA, which is summarized in Algorithm 2.

V. PERFORMANCE EVALUATION

In this section, we evaluate the performance of our proposed algorithms by using the real experimental dataset [15] from the SPAN Lab of the University of Utah. All algorithms are realized in MATLAB® 2016a and executed on a Windows 64-bit computer with 8GB RAM and Intel(R) Core(TM) i7 CPU.

A. PHYSICAL DESCRIPTION OF EXPERIMENT

As illustrated in Fig. 8, we can see that the experiments were carried out with the following settings: 28 wireless sensor nodes were deployed in a square perimeter of a 21x21 foot square, each node was spaced 3 feet from the neighboring nodes and was placed on a stand at 3 feet off the ground. The black stars represent the RPs (i.e. reference points) of which total number is 35. In addition, the monitoring area contains two trees with a circumference of approximately three feet. In the experiment, we consider the dataset [15] with the target that is a person with the height 1.85 m and the weight 88 kg. TelosB wireless sensor nodes are made by Crossbow. Each node works in the 2.4GHz frequency band and uses the IEEE

Algorithm 2 SSC-ISTA

Require: $\mathbf{y} \in \mathbf{R}^m$, $\mathbf{W} \in \mathbf{R}^{m \times n}$, ρ, $\boldsymbol{\beta}_0 = \mathbf{0}$, $\mathbf{I} = \mathbf{1}$, C
Ensure: φ or $\{\varphi_1, \ldots, \varphi_N\}$

```
Perform SVD procedure and conduct transformation in the direction of column-dimension, according to (20)-(22)
Choose C(C >largest eigenvalue of U_norm^T U_norm ïijL; θ ← ρ/C
Perform EVD procedure and conduct dimensionality reduction in the direction of row-dimension, according to (23)-(28)
for i = 0 to maxiteration do
    β_{i+1} = h_θ((1/C) W_appr^T y_appr + (I − (1/C) W_appr^T W_appr) β_i)
    Until ||β_{i+1} − β_i||_2^2 below a threshold
end for
β* ← β_{i+1}
if locate single target then
    Determine φ by (31)
    Return φ
end if
if locate sparse N multi-targets then
    Determine φ_1, ..., φ_N by (32)
    Return {φ_1, ..., φ_N}
end if
```

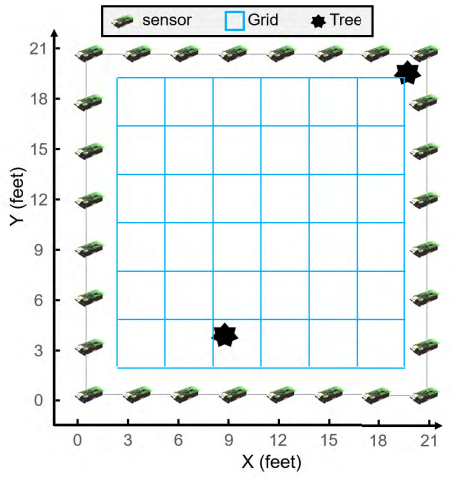

FIGURE 8. Illustration of DFL experiment setup according to the SPAN Lab of the University of Utah [15]. Here, RP is the reference point.

802.15.4 standard for communication. A base station node listens to the whole network traffic, and then delivers the collected data to a computer via a USB port.

At each RP, 30 trials had been conducted with a short time interval. Since one grid of coordinate (9, 6) has no corresponding data, in our performance evaluation, 35 RPs are selected as testing positions. Meanwhile, total RSS sample matrices of each RP are divided into two portions, which 25 trials are used to construct dictionary, and then the mean of the remaining 5 ones is used as testing signals for locating single target; for locating multi-targets, the case of locating two targets is taken as the example, where the dictionary is same with that of locating single target, while testing signals are from other 30 new RSS samples.

B. EXPERIMENTAL RESULTS

In this section, we present numerical experiment results to evaluate the performance of SC-ISTA and SSC-ISTA. The outline is as follows: items 1), 2) and 3) of section V-B, show the performance for locating single target; item 4) of section V-B shows the performance for locating two targets; item 5) of section V-B shows the time cost for sparse coding; item 6) of section V-B compares the localization performance with [19]. Description of experiment setting is as follows,

Compared Approaches: In order to conveniently describe the advantage of the proposed SC-ISTA and SSC-ISTA, three efficient algorithms are used to compare the localization performance with the proposed approaches. Among the compared algorithms, deep learning with autoencoder (**DL-AE**) and K-nearest-neighbor (**KNN**), the state-of-the-art methods for DFL [16], [53], [54], are used as the classifiers for comparison. The third one is the **OMP**, an effective sparse-coding-based algorithm for DFL [40]. All of the compared algorithms are commonly used in DFL. For simplicity, we abbreviate the OMP of applying SSC-scheme to the **SSC-OMP** in the following description.

Other Settings and Metrics: In order to make the presentation clarity, some performance metrics are given as:

- Suppose that C_{total} is the total number of testing samples, and $C_{correct}$ is the number of samples that can be correctly located. Then the localization accuracy is calculated by

$$Accuracy = \frac{C_{correct}}{C_{total}} \tag{33}$$

- Suppose that the N targets are with true locations $(x_1, y_1), \ldots, (x_N, y_N)$, and the corresponding estimated locations are $(x'_1, y'_1), \ldots, (x'_N, y'_N)$. The performance metric is the mean localization error (MLE), the mean distance between the true location and the estimated location of N targets, which is expressed as

$$MLE = \frac{\sum_{l=1}^{N} \sqrt{(x_l - x'_l)^2 + (y_l - y'_l)^2}}{N} \tag{34}$$

  Specifically, when N = 1, i.e., for locating a single target, the MLE in this paper is called localization error (LE) $e_i (1 \le i \le 35)$ which is the Euclidean distance between the estimated position and the true position of a target at the i-th RP; and then, average localization error (ALE) is defined as $\sum_{i=1}^{35} e_i/35$, which is calculated after target passes through all RPs.

The Accuracy, MLE, LE, and ALE are used to evaluate the localization accuracy of algorithms.

In practical application, the DFL system will be affected unavoidably. In order to evaluate the performance of our algorithms under different additive noises, we simulated the additive noise with the Gaussian distribution. Taking the i-th

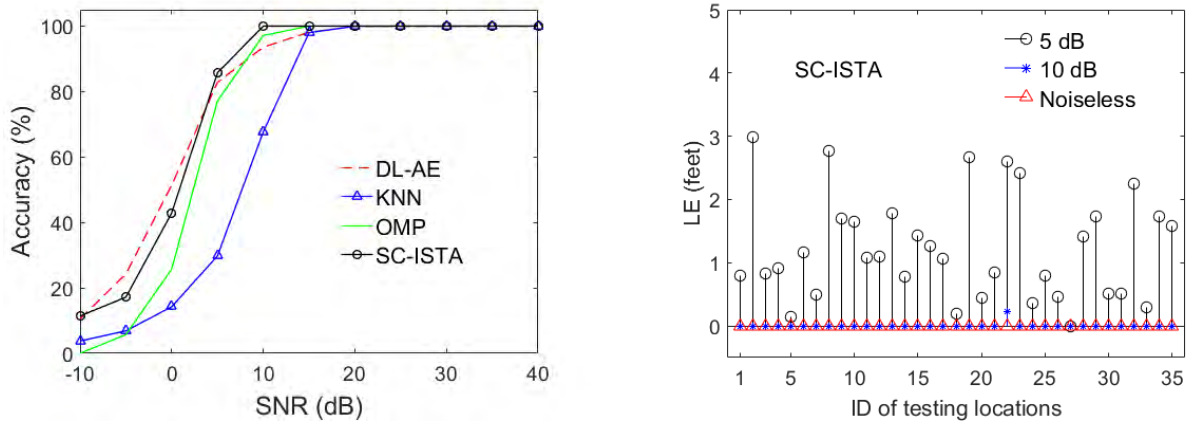

(a) (b)

FIGURE 9. Localization performance of the proposed SC-ISTA with the noisy and the noiseless testing signal. (a) Accuracy of the proposed SC-ISTA and the compared methods. (b) Localization error (LE) of SC-ISTA for each locations.

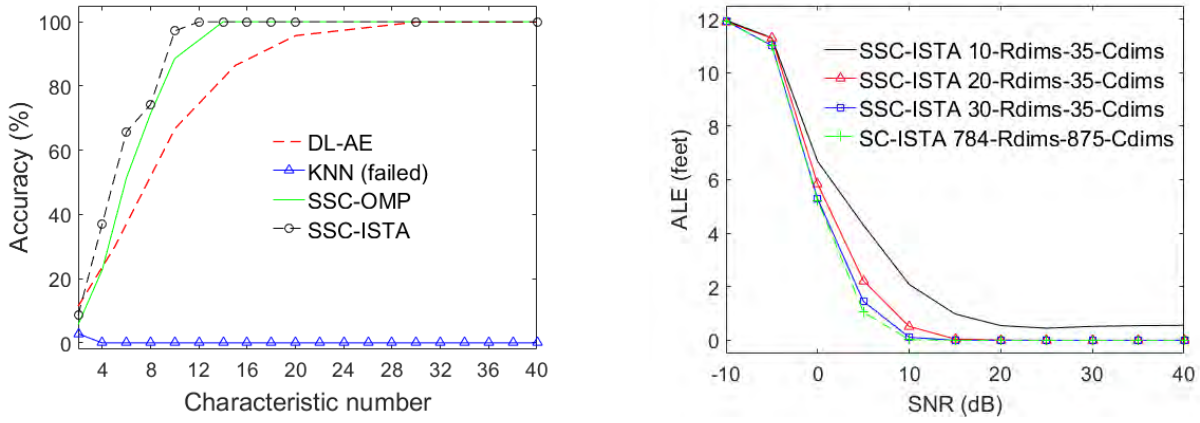

(a) (b)

FIGURE 10. Localization performance of the proposed SSC-ISTA and the compared methods with different low dimensional data. Here, the characteristic number is associated with the row dimensions (Rdims). (a) Accuracy of the proposed SSC-ISTA and the compared methods. (b) Average localization errors (ALE) of 10, 20, 30-Rdims-35-Cdims and 784-Rdims-875-Cdims under SNR ranging from −10 dB to 40 dB.

RP ($1 \leq i \leq 35$) as an example, the noises are added into testing signal matrix $\mathbf{S}_i$ as well as the dictionary $\mathbf{D}$, by the way of $\mathbf{S}_i^* = \mathbf{S}_i + \mathbf{N}$ and $\mathbf{D}^* = \mathbf{D} + \mathbf{N}$. Here $\mathbf{N}$ is a Gaussian noise matrix that obeys the Gaussian distribution. A common measure for signal quality under noisy environment is the SNR, in our experiments, the SNR of testing signal is set to vary from −10 dB to 40 dB, and then the SNR of the dictionary is set to vary from 0 dB to 40 dB.

1) LOCALIZATION PERFORMANCE OF SC-ISTA

The localization performances of the proposed SC-ISTA and the compared DFL methods, including DL-AE, KNN and OMP, are shown in Fig. 9. From Fig. 9(a), when SNR is greater than 10 dB, the accuracy can be basically achieved by 100% which is very high. It is clear to see that the accuracy of our proposed SC-ISTA algorithms is higher than the other three algorithms when the testing signal is noisy with SNR greater than 5 dB. When SNR is smaller than 5 dB, the accuracies of all algorithms are decreased sharply, which indicates the performance degradation of the localization. In addition, Fig. 9(a) shows that the proposed SC-ISTA outperforms another sparse-coding-based algorithm, OMP. Fig. 9(b) shows the LE of SC-ISTA under noise from −10 dB to 40 dB. It can be seen that the LEs of all testing locations approach 0 feet under the SNR conditions 10 dB and the noiseless case. It indicates that the proposed SC-ISTA algorithm is highly accurate and robust to noise when SNR is greater than 10 dB.

2) LOCALIZATION PERFORMANCE OF SSC-ISTA WITH DATA REDUCED DIMENSIONS FROM HIGH 784-RDIMS-875-CDIMS TO LOW DIMS

In this part of experiments, the column dimensions are reduced to the same dimensions of 35-Cdims for SSC-ISTA, the row dimensions are reduced to different Rdims, as shown in Fig. 10. The localization performances of the proposed SSC-ISTA and the compared algorithms are evaluated in the same dimension-number of subspace. From Fig. 10(a), it can be seen that the proposed SSC-ISTA outperforms the other three algorithms. When the row dimensions are reduced to

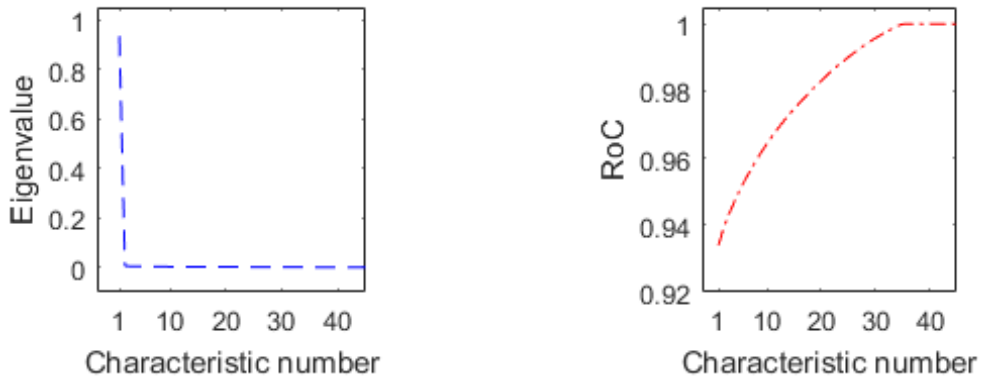

FIGURE 11. Eigenvalue and ratio of cumulative distribution (RoC) associated with the characteristics from the 1-st one to the 40-th one. (a) Eigenvalue. (b) Ratio of the cumulative distribution.

10-Rdims, the accuracy of SSC-ISTA can be achieved to 97.1% which is higher than the other three methods; When the row dimensions are 12-Rdims, the accuracy is 100% but the convergence speed is faster than other three methods. When the row dimensions are er than 10-Rdims, the accuracies of these four algorithms are lower than 95% which is not good for localization. Fig. 10(b) shows the comparison of SC-ISTA and SSC-ISTA for ALE and robustness under SNR from -10 dB to 40 dB when the data are of different dimensions. It can be seen that, when SNR is greater than 10 dB, ALE of SC-ISTA approaches 0 feet and the same case is with SSC-ISTA of 30-Rdims. It is worth noting that, when SNR is greater than 15 dB, the SSC-ISTA of 20-Rdims also performs well. It indicates that the localization accuracy and robustness are not decreased by reducing the dimensions to 30-Rdims-35-Cdims, the SSC-ISTA works well with the dimension-reduced data and is robust to the noisy environment when SNR is greater than 10 dB.

This means that even the dimension of DFL data is reduced from a high 784-Rdims-875-Cdims to the low 20-Rdims-35-Cdims of noiseless, or 30-Rdims with SNR greater than 10 dB, SSC-ISTA still works effectively and keeps a high accuracy, which will drastically lighten the computing burden.

The reason why low-dimension data can be used in DFL is that, through the EVD procedure, almost all of the important features of each class are extracted into an eigenvector. Thus, the main features are not lost after reducing the column dimensions. And then, through the SVD decomposition, as shown in Fig. 11(a), eigenvalues associated with original data are classified and sorted descending. In such a case, the eigenvalues are in descending order, the first principal component $\mathbf{u}_1$ represents the characteristic of the maximum variance in the DFL data, and the second principal component $\mathbf{u}_2$ represents the characteristic of the sub-maximum variance in the DFL data, and so on. After the SVD procedure, according to the calculated result, as shown in Fig. 11(b), the approximate 97 percent of main characteristics are moved to the former 12-Rdims and the other 3 percent of unimportant characteristics are moved to the latter Rdims, and the noise is included in the latter unimportant characteristics and rejected from the dataset. Thus, we can see that, in Fig. 10(a), when the characteristic number is higher than 12, the accuracy can be achieved to 100%, showing a good localization performance. Mainly because the top 12 characteristics of dimension-reduced data can be able to represent 97 percent of characteristics of the original dataset, which are enough to guarantee the precision for DFL application.

From Fig. 10, it can be seen that, during SNR greater than 10 dB, the accuracy and ALE of 30-Rdims-35-Cdims show the same good localization performance compared with 784-Rdims-875-Cdims. Hence, we chose the 30-Rdims-35-Cdims of dimension-reduced data to do the following experiments.

3) LOCALIZATION PERFORMANCE OF SC-ISTA AND SSC-ISTA WITH THE NOISE DICTIONARY AND THE NOISY TESTING SIGNAL

In the above mentioned item 1) and 2) of section V-B, the performances of all algorithms are evaluated under the case that noise appears in the testing stage. In this subsection, the performance of SC-ISTA and SSC-ISTA are evaluated under the condition that noise appears both of the testing stage as well as the stage of constructing the dictionary.

As shown in Fig. 12, regarding the datasets of the original 784-Rdims-875-Cdims and the 30-Rdims-35-Cdims, the noise from 0 dB to 40 dB with an interval of 5 dB are respectively added into dictionaries. At the same time, the testing datasets with SNR $=$ 10 dB and SNR $=$ 20 dB as well as noiseless dataset are used. From Fig. 12(a), it can be seen that, when input the noiseless testing signals or the noisy ones of SNR $=$ 20 dB, the SC-ISTA can be achieved with a high accuracy that ALE is 0 feet and be robust to SNR of 15 dB; when the noisy testing signals of SNR $=$ 10 dB are input, SC-ISTA can be achieved a high accuracy until the SNR of dictionary is greater than 25 dB.

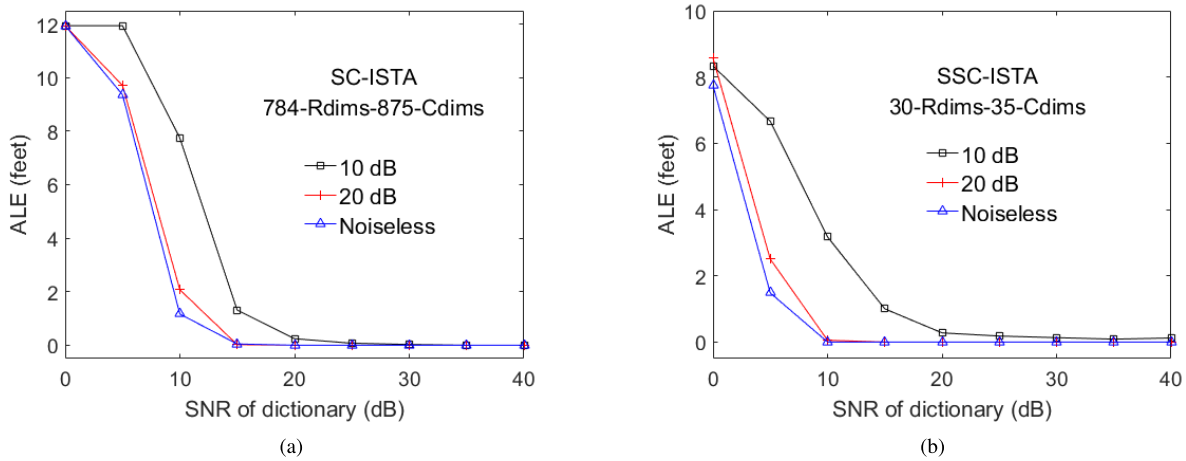

FIGURE 12. Localization performance of SC-ISTA and SSC-ISTA with the noisy dictionary when the testing signal is noisy with SNR = 10 dB and 20 dB as well as the case of noiseless. (a) Average localization errors of SC-ISTA. (b) Average localization errors of SSC-ISTA.

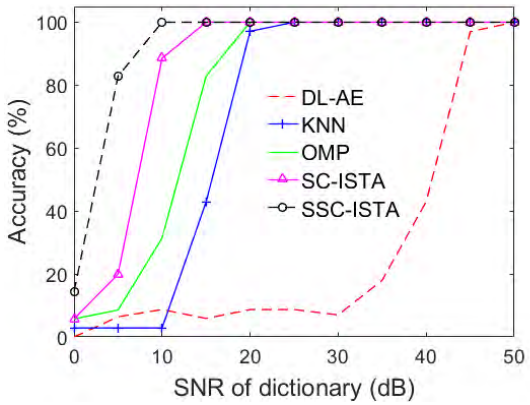

FIGURE 13. Accuracy of the proposed approaches and the compared methods with the noiseless testing signal. For the SSC-ISTA is with 30-Rdims-35-Cdims and the others are with 784-Rdims-875-Cdims.

From Fig. 12(b), it can be seen that, when input the noiseless testing signals or the noisy ones of SNR = 20 dB, the SSC-ISTA can be maintained a high accuracy that ALE is 0 feet and is robust until the SNR of dictionary reaches 10 dB. Whereas, when the noise level of the testing signal reaches SNR = 10 dB, SSC-ISTA cannot maintain the high accuracy and is not robust. It is worthy of note that, when the SNR of the dictionary is 10 dB, the accuracy of SSC-ISTA is higher than SC-ISTA, mainly because the EVD is actually a procedure of feature extraction and denoising, the reason has been detailedly discussed in item 2) of section V-B.

From Fig. 13, the proposed SSC-ISTA and SC-ISTA outperform the other three DFL algorithms, and the SSC-ISTA outperforms SC-ISTA with the noisy dictionary.

Hence, even the dataset are destroyed by noise with a certain level in the stage of constructing dictionary and testing stage, both of SC-ISTA and SSC-ISTA can maintain good performance in terms of accuracy and robustness.

4) LOCALIZATION PERFORMANCE OF SC-ISTA AND SSC-ISTA FOR LOCATING MULTI-TARGETS

In this subsection, the localization performances of SC-ISTA and SSC-ISTA are evaluated for locating multi-targets, where the case of locating two targets is taken as the example. Six cases of two targets' locations are listed in Table 3. The performance metrics are MLE and ALE, which are given in beginner of the Section V-B. The localization result is shown in Fig. 14.

TABLE 3. Six cases of two targets' locations.

Cases	Coordinate (Unit: feet)	
	Target 1 (x_1, y_1)	Target 2 (x_2, y_2)
1	(3, 15)	(6, 15)
2	(3, 15)	(9, 15)
3	(3, 15)	(12, 15)
4	(3, 15)	(15, 15)
5	(3, 15)	(18, 15)
6	(3, 15)	(15, 12)

From Fig. 14(b), when the SC-ISTA is with the dictionary of 784-Rdims-875-Cdims, the mean localization errors of former 5 cases are all zero, which means that locations of two targets can be estimated exactly. For the 6-th case, the target 1 is located exactly, but, the target 2 is located at its adjacent position of (12, 15), which results in a localization error of 2.1 feet. For the SSC-ISTA, When it is with the low dimensional dictionary of 15-Rdims-35-Cdims, a big error of the 6-th case and a error are existed in the 3-rd case; when it is with the dictionary of 20-Rdims-35-Cdims, localization error of the 6-th case is obviously reduced. Moreover, when the dictionary of 25-Rdims-35-Cdims is used, all of the errors disappear except for a error of the 6-th case, which achieves the same accuracy with SC-ISTA. From Fig. 14(b), it is shown that the proposed SSC-ISTA outperforms the other three DFL

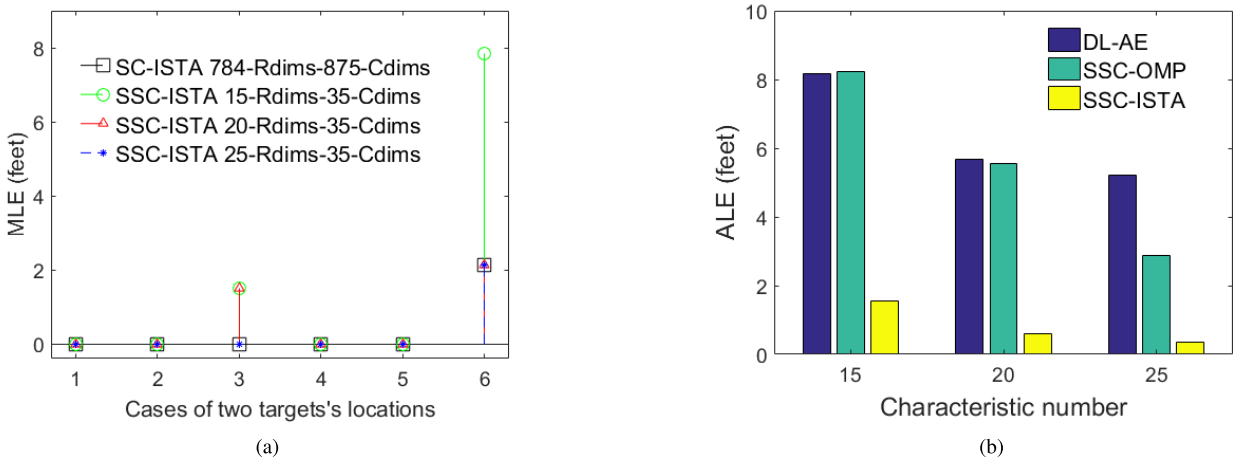

FIGURE 14. Localization performance of the proposed SC-ISTA, SSC-ISTA and the compared approaches for locating two targets. (a) Mean localization error (MLE) of SC-ISTA and SSC-ISTA. For the 6-th case of SC-ISTA and SSC-ISTA-25-Rdims, the MLE is resulted from the target 2 that is estimated at the location of (12, 15). (b) Average localization error (ALE) of SSC-ISTA and the compared approaches with the data of 15-Rdims-35-Cdims, 20-Rdims-35-Cdims and 25-Rdims-35-Cdims, respectively. KNN was failed to locate multi-targets.

algorithms with the data of 15-Rdims-35-Cdims, 20-Rdims-35-Cdims and 25-Rdims-35-Cdims.

Therefore, Fig. 14 indicates that, when used to locate two targets, the SC-ISTA can achieve a high localization accuracy as well as the SSC-ISTA with the data of 25-Rdims-35-Cdims.

5) TIME COST OF THE PROPOSED SC-ISTA AND SSC-ISTA WITH THE DIFFERENTLY DIMENSIONAL DATA

In this section, experiments are performed to test the execution time for sparse coding with the sparse-coding-based algorithms, including OMP, SSC-OMP, SC-ISTA, and SSC-ISTA, when faced data with different dimensions.

The experiment results are shown in Table 4, which shows the time cost for sparse coding when faced high-dimension data, and their accelerating effect when input data is reduced from the high 784-Rdims-875-Cdims to the low dimensions.

TABLE 4. Time cost of DFL algorithms when the input data are with different dimensions.

Methods for sparse coding	Dimensions of dictionary	Sparse coding time(s)
OMP	784-Rdims-875-Cdims	0.4
SC-ISTA	784-Rdims-875-Cdims	2.1×10^{-3}
SSC-OMP	30-Rdims-35-Cdims	3.7×10^{-4}
SSC-ISTA	30-Rdims-35-Cdims	2.1×10^{-4}

From Table 4, when input data is 784-Rdims-875-Cdims without dimension reduction, the time costs of OMP and the proposed SC-ISTA for sparse coding are 0.4 s and 2.1×10^{-3} s, respectively, which indicates that the proposed SC-ISTA is much more efficient than OMP with the high-dimensional DFL data. Then, after reducing dimensions to 30-Rdims-35-Cdims, the time costs are drastically reduced to 3.7×10^{-4} s, 2.1×10^{-4} s, which means that the two algorithms are all significant accelerated and their time costs are highly reduced, and the proposed SSC-ISTA is much more efficient than SSC-OMP.

It is worth noting that, since the proposed algorithms are very fast, it is possible to be directly applied in tracking the moving target, i.e. a real-time online processing.

6) ADDITIONAL DISCUSSION ON THE EFFECTIVENESS OF THE PROPOSED APPROACH AND THE BP-LP

Reference [19] share some similarities in a certain sense. In order to present the advantages of the proposed approach, some contrastive experiments were conducted. Our experiment results are shown in the following Fig. 15 and Table 5. From Fig. 15, it can be seen that the accuracies of the proposed SC-ISTA and SSC-ISTA are slightly higher than the BP-LP algorithm. Moreover, in Table 5, the efficiencies of the proposed SC-ISTA and SSC-ISTA are much higher than the BP-LP. In particular, when input the high-dimensional data with 784-Rdims-875-Cdims, SC-ISTA is far faster than BP-LP. Even though the dimensions of the dictionary are reduced from 784-Rdims-875-Cdims to 30-Rdims-35-Cdims, SSC-ISTA is still one hundred times faster than BP-LP. It is worthy of note that, the SSC-BP-LP algorithm is based on our SSC-scheme, which leads to a significant acceleration for the BP-LP. However, [19] applies the BP-LP that does not utilize the proposed SSC-scheme, therefore the localization process would be very slow, which results in not applicable for real-time detecting or tracking target.

It should be noticed that our work and [19] share some similarities in a certain sense as the reviewer mentioned, but there are several important distinct features that are different in our work. For example, [19] just focuses on the application for locating a single target. Whereas, in our manuscript, we systematically formulate and proof that the proposed

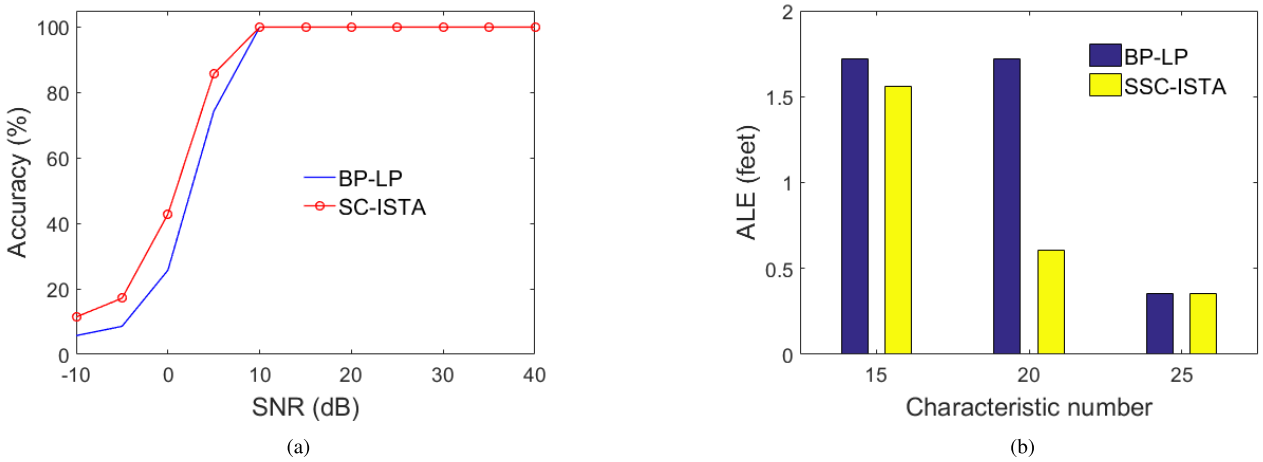

FIGURE 15. The comparison of the proposed approach and BP-LP with respect to the localization performance. (a) Accuracy of BP-LP and the proposed SC-ISTA with the noisy testing signal for locating single target. (b) Accuracy of BP-LP and the proposed SC-ISTA with the noisy testing signal for locating.

TABLE 5. Comparison of the proposed approach and BP-LP with respect to the efficiency.

Methods for sparse coding	Dimensions of dictionary	Sparse coding time(s)
BP-LP	784-Rdims-875-Cdims	33.9
SSC-BP-LP	30-Rdims-35-Cdims	1.8×10^{-2}

approach is applicable for locating multi-targets by a single test signal, and this is quite important in the DFL field.

VI. CONCLUSION

In order to achieve an accurate and efficient process for DFL, we formulated DFL as an SRC problem, presented a sparse model, and conducted sparse coding in signal subspace for target Localization, which led to the algorithms of SC-ISTA and SSC-ISTA in the signal subspace.

Experimental results showed that: in the task for locating a single target, the proposed SC-ISTA was able to achieve a high localization accuracy of 100% and was robust up to SNR $=$ 10 dB for the noisy testing data. And then, the proposed SSC-ISTA could maintain the same high accuracy of 100% when the noiseless data were reduced from 784-Rdims-875-Cdims to 12-Rdims-35-Cdims, and was also robust to the noisy case of SNR $=$ 10 dB when it was with the data of 30-Rdims-35-Cdims. When noise appeared in the stage of constructing dictionary, both the SC-ISTA and the SSC-ISTA could keep the good performance. For the noisy testing signal with SNR $=$ 10 dB, the SC-ISTA was robust to the noisy dictionary with SNR $=$ 25 dB; for the noisy testing signal with SNR higher than 20 dB, the SC-ISTA was robust to the noisy dictionary with SNR $=$ 15 dB and the SSC-ISTA can be robust to SNR $=$ 10 dB. In the task of locating multi-targets, the SC-ISTA could achieve a high localization accuracy as well as the SSC-ISTA with the data of 25-Rdims-35-Cdims.

Finally, we compared the localization performance of the proposed approaches with three other algorithms, including DL-AE, KNN and OMP which are commonly used in localization. Experimental results showed that the proposed SC-ISTA and SSC-ISTA outperformed these three algorithms in this DFL application. Moreover, the sparse coding time of the proposed algorithms was 2.1×10^{-3} and 2.1×10^{-4} which was much lower than another sparse-coding-based algorithm, OMP, no matter before and after utilizing the SSC-scheme. It indicated that the proposed approaches are promising to be used in tracking motionless or moving targets, for example, for detecting locations and activities of old people and patients at home or in the hospitals, location-based services in shopping centers etc., as well as for detecting intruders' locations and tracking in security safeguard.

REFERENCES

[1] M. Akter, O. Rahman, N. Islam, M. M. Hassan, A. Alsanad, and A. K. Sangaiah, "Energy-efficient tracking and localization of objects in wireless sensor networks," *IEEE Access*, vol. 6, pp. 17165–17177, 2018.

[2] T.-H. Chiang, Y.-T. Chuang, C.-L. Ke, L.-J. Chen, and Y.-C. Tseng, "Calorie map: An activity intensity monitoring system based on wireless signals," in *Proc. IEEE Wireless Commun. Netw. Conf. (WCNC)*, Mar. 2017, pp. 1–6.

[3] B. Liu, W. Zhou, T. Zhu, L. Gao, T. H. Luan, and H. Zhou, "Silence is golden: Enhancing privacy of location-based services by content broadcasting and active caching in wireless vehicular networks," *IEEE Trans. Veh. Technol.*, vol. 65, no. 12, pp. 9942–9953, Dec. 2016.

[4] W. M. Y. W. Bejuri, M. M. Mohamad, R. Zahilah, and R. Z. R. M. Radzi, "Emergency rescue localization (ERL) using GPS, wireless LAN and camera," *Int. J. Softw. Eng. Appl.*, vol. 9, no. 9, pp. 217–232, 2015.

[5] K. Akkaya, I. Guvenc, R. Aygun, N. Pala, and A. Kadri, "IoT-based occupancy monitoring techniques for energy-efficient smart buildings," in *Proc. IEEE Wireless Commun. Netw. Conf. Workshops (WCNCW)*, Mar. 2015, pp. 58–63.

[6] F. Yucel and E. Bulut, "Clustered crowd GPS for privacy valuing active localization," *IEEE Access*, vol. 6, pp. 23213–23221, 2018.

[7] C. Whitelam and T. Bourlai, "Accurate eye localization in the short waved infrared spectrum through summation range filters," *Comput. Vis. Image Understand.*, vol. 139, pp. 59–72, Oct. 2015.

[8] C. Medina, J. C. Segura, and A. De la Torre, "Ultrasound indoor positioning system based on a low-power wireless sensor network providing sub-centimeter accuracy," *Sensors*, vol. 13, no. 3, pp. 3501–3526, 2013.
[9] K. Pahlavan, P. Krishnamurthy, and Y. Geng, "Localization challenges for the emergence of the smart world," *IEEE Access*, vol. 3, pp. 3058–3067, Dec. 2015.
[10] R. Harle, "A survey of indoor inertial positioning systems for pedestrians," *IEEE Commun. Surveys Tuts.*, vol. 15, no. 3, pp. 1281–1293, Jul. 2013.
[11] J. Xiao, Z. Zhou, Y. Yi, and L. M. Ni, "A survey on wireless indoor localization from the device perspective," *ACM Comput. Surv.*, vol. 49, no. 2, p. 25, 2016.
[12] L. Chang *et al.*, "FitLoc: Fine-grained and low-cost device-free localization for multiple targets over various areas," *IEEE/ACM Trans. Netw.*, vol. 25, no. 4, pp. 1994–2007, Aug. 2017.
[13] Y. Guo, K. Huang, N. Jiang, X. Guo, Y. Li, and G. Wang, "An exponential-Rayleigh model for RSS-based device-free localization and tracking," *IEEE Trans. Mobile Comput.*, vol. 14, no. 3, pp. 484–494, Mar. 2015.
[14] O. Kaltiokallio, H. Yigitler, and R. Jäntti, "A three-state received signal strength model for device-free localization," *IEEE Trans. Veh. Technol.*, vol. 66, no. 10, pp. 9226–9240, Oct. 2017.
[15] J. Wilson and N. Patwari, "Radio tomographic imaging with wireless networks," *IEEE Trans. Mobile Comput.*, vol. 9, no. 5, pp. 621–632, May 2010.
[16] J. Wang, X. Zhang, Q. Gao, H. Yue, and H. Wang, "Device-free wireless localization and activity recognition: A deep learning approach," *IEEE Trans. Veh. Technol.*, vol. 66, no. 7, pp. 6258–6267, Jul. 2017.
[17] S. Sahin, H. Ozcan, and K. Kucuk, "Smarttag: An indoor positioning system based on smart transmit power scheme using active tags," *IEEE Access*, vol. 6, pp. 23500–23510, 2018.
[18] Q. Lei, H. Zhang, H. Sun, and L. Tang, "A new elliptical model for device-free localization," *Sensors*, vol. 16, no. 4, p. 577, 2016.
[19] D. S. Wang, X. S. Guo, and Y. X. Zou, "Accurate and robust device-free localization approach via sparse representation in presence of noise and outliers," in *Proc. IEEE Int. Conf. Digit. Signal Process. (DSP)*, Oct. 2016, pp. 199–203.
[20] J.-W. Yoon and T. Park, "Maximizing localization accuracy via self-configurable ultrasonic sensor grouping using genetic approach," *IEEE Trans. Instrum. Meas.*, vol. 65, no. 7, pp. 1518–1529, Jul. 2016.
[21] Z. Li, S. Ding, and Y. Li, "A fast algorithm for learning overcomplete dictionary for sparse representation based on proximal operators," *Neural Comput.*, vol. 27, no. 9, pp. 1951–1982, 2015.
[22] Z. Li, "Efficient learning algorithms for overcomplete dictionaries for sparse representation of signal," Ph.D. dissertation, Univ. Aizu, Aizuwakamatsu, Japan, 2015.
[23] L. Yan and Y. Kongyu, "Immunity genetic algorithm based on elitist strategy and its application to the TSP problem," in *Proc. Int. Symp. Intell. Inf. Technol. Appl. Workshops (IITAW)*, 2008, pp. 3–6.
[24] J. Liu, N. An, M. T. Hassan, M. Peng, Z. Cui, and S. Zhao, "Redundancy reduction for indoor device-free localization," *Pers. Ubiquitous Comput.*, vol. 21, no. 1, pp. 5–15, Feb. 2017.
[25] Z. Wang, H. Liu, S. Xu, X. Bu, and J. An, "Bayesian device-free localization and tracking in a binary RF sensor network," *Sensors*, vol. 17, no. 5, p. 969, 2017.
[26] J. Wang, Q. Gao, H. Wang, P. Cheng, and K. Xin, "Device-free localization with multidimensional wireless link information," *IEEE Trans. Veh. Technol.*, vol. 64, no. 1, pp. 356–366, Jan. 2015.
[27] M. Youssef, M. Mah, and A. Agrawala, "Challenges: Device-free passive localization for wireless environments," in *Proc. 13th Annu. ACM Int. Conf. Mobile Comput. Netw.*, 2007, pp. 222–229.
[28] M. Moussa and M. Youssef, "Smart cevices for smart environments: Device-free passive detection in real environments," in *Proc. IEEE Int. Conf. Pervas. Comput. Commun. (PerCom)*, Mar. 2009, pp. 1–6.
[29] I. Sabek, M. Youssef, and A. V. Vasilakos, "ACE: An accurate and efficient multi-entity device-free WLAN localization system," *IEEE Trans. Mobile Comput.*, vol. 14, no. 2, pp. 261–273, Feb. 2015.
[30] D. Zhang, J. Ma, Q. Chen, and L. M. Ni, "An RF-based system for tracking transceiver-free objects," in *Proc. 5th Annu. IEEE Int. Conf. Pervas. Comput. Commun. (PerCom)*, Mar. 2007, pp. 135–144.
[31] D. Zhang, Y. Liu, X. Guo, and L. M. Ni, "RASS: A real-time, accurate, and scalable system for tracking transceiver-free objects," *IEEE Trans. Parallel Distrib. Syst.*, vol. 24, no. 5, pp. 996–1008, May 2013.
[32] J. Wang, Q. Gao, H. Wang, Y. Yu, and M. Jin, "Time-of-flight-based radio tomography for device free localization," *IEEE Trans. Wireless Commun.*, vol. 12, no. 5, pp. 2355–2365, May 2013.
[33] J. Wang, D. Fang, X. Chen, Z. Yang, T. Xing, and L. Cai, "LCS: Compressive sensing based device-free localization for multiple targets in sensor networks," in *Proc. IEEE INFOCOM*, Apr. 2013, pp. 145–149.
[34] B. Mager, P. Lundrigan, and N. Patwari, "Fingerprint-based device-free localization performance in changing environments," *IEEE J. Sel. Areas Commun.*, vol. 33, no. 11, pp. 2429–2438, Nov. 2015.
[35] M. Seifeldin, A. Saeed, A. E. Kosba, A. El-Keyi, and M. Youssef, "Nuzzer: A large-scale device-free passive localization system for wireless environments," *IEEE Trans. Mobile Comput.*, vol. 12, no. 7, pp. 1321–1334, Jul. 2013.
[36] B. Molina, E. Olivares, C. E. Palau, and M. Esteve, "A multimodal fingerprint-based indoor positioning system for airports," *IEEE Access*, vol. 6, pp. 10092–10106, 2018.
[37] W. Xiao, B. Song, X. Yu, and P. Chen, "Nonlinear optimization-based device-free localization with outlier link rejection," *Sensors*, vol. 15, no. 4, pp. 8072–8087, 2015.
[38] M. Grant, S. Boyd, and Y. Ye. (2009). *CVX Users' Guide*. [Online]. Available: http://cvxr.com/cvx/cvxusrguide.pdf
[39] J. Wang, X. Feng, Q. Gao, X. Zhang, and M. Jin, "FM-based device-free localization and activity recognition via sparse representation," in *Proc. 1st Workshop Context Sens. Activity Recognit.*, 2015, pp. 7–12.
[40] T. Liu, X. Luo, and Z. Liang, "Enhanced sparse representation-based device-free localization with radio tomography networks," *J. Sens. Actuator Netw.*, vol. 7, no. 1, p. 7, 2018.
[41] Y. Zhao and N. Patwari, "Noise reduction for variance-based device-free localization and tracking," in *Proc. 8th Annu. IEEE Commun. Soc. Conf. Sensor, Mesh Ad Hoc Commun. Netw. (SECON)*, Jun. 2011, pp. 179–187.
[42] J. Han, D. Zhang, G. Cheng, N. Liu, and D. Xu, "Advanced deep-learning techniques for salient and category-specific object detection: A survey," *IEEE Signal Process. Mag.*, vol. 35, no. 1, pp. 84–100, Jan. 2018.
[43] X. Yao, J. Han, D. Zhang, and F. Nie, "Revisiting co-saliency detection: A novel approach based on two-stage multi-view spectral rotation co-clustering," *IEEE Trans. Image Process.*, vol. 26, no. 7, pp. 3196–3209, Jul. 2017.
[44] G. Cheng, C. Yang, X. Yao, L. Guo, and J. Han, "When deep learning meets metric learning: Remote sensing image scene classification via learning discriminative CNNs," *IEEE Trans. Geosci. Remote Sens.*, vol. 56, no. 5, pp. 2811–2821, May 2018.
[45] T. Van Haute, B. Verbeke, E. De Poorter, and I. Moerman, "Optimizing time-of-arrival localization solutions for challenging industrial environments," *IEEE Trans. Ind. Informat.*, vol. 13, no. 3, pp. 1430–1439, Jun. 2017.
[46] J. Wright, A. Y. Yang, A. Ganesh, S. S. Sastry, and Y. Ma, "Robust face recognition via sparse representation," *IEEE Trans. Pattern Anal. Mach. Intell.*, vol. 31, no. 2, pp. 210–227, Feb. 2009.
[47] D. L. Donoho and M. Elad, "Optimally sparse representation in general (nonorthogonal) dictionaries via $\ell 1$ minimization," *Proc. Nat. Acad. Sci. USA*, vol. 100, no. 5, pp. 2197–2202, 2003.
[48] E. J. Candès and T. Tao, "Near-optimal signal recovery from random projections: Universal encoding strategies?" *IEEE Trans. Inf. Theory*, vol. 52, no. 12, pp. 5406–5425, Dec. 2006.
[49] A. Beck and M. Teboulle, "A fast iterative shrinkage-thresholding algorithm for linear inverse problems," *SIAM J. Imag. Sci.*, vol. 2, no. 1, pp. 183–202, 2009.
[50] L. I. Smith, "A tutorial on principal components analysis," Tech. Rep., 2002. [Online]. Available: http://www.cs.otago.ac.nz/cosc453/student_tutorials/principal_components.pdf
[51] L. Zhang, W. Dong, D. Zhang, and G. Shi, "Two-stage image denoising by principal component analysis with local pixel grouping," *Pattern Recognit.*, vol. 43, no. 4, pp. 1531–1549, 2010.
[52] A. A. Miranda, Y.-A. Le Borgne, and G. Bontempi, "New routes from minimal approximation error to principal components," *Neural Process. Lett.*, vol. 27, no. 3, pp. 197–207, 2008.
[53] X. Zhang, J. Wang, Q. Gao, X. Ma, and H. Wang, "Device-free wireless localization and activity recognition: A deep learning approach," in *Proc. IEEE Int. Conf. Pervas. Comput. Commun. Workshops (PerCom Workshops)*, 2016, pp. 1–5.
[54] D. A. Tran, S. Gong, and Q. Vo, "Geometric-based KNN localization using sensor dissimilarity information," in *Proc. IEEE 28th Annu. Int. Symp. Pers., Indoor, Mobile Radio Commun. (PIMRC)*, Oct. 2017, pp. 1–6.

HUAKUN HUANG received the B.Sc. and M.Sc. degrees from Guangzhou University, Guangzhou, China, in 2014 and 2016, respectively. He is currently pursuing the Ph.D. degree with the School of Computer Science and Engineering, The University of Aizu, Japan. His current research interests include signal processing, sparse representation, optimization, machine learning, and their applications, e.g., localization, image processing, and pattern recognition.

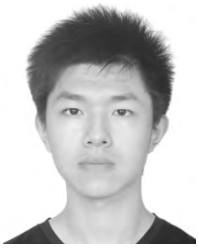

HAOLI ZHAO received the B.Sc. degree in nuclear physics from the College of Physical Science and Technology, Sichuan University, China, in 2012, and the M.Sc. degree in nuclear environmental science and technology from the Department of Material, Sheffield University, England, U.K., in 2014. He is currently pursuing the Ph.D. degree with the Graduate Department of Computer and Information System, The University of Aizu, Japan. His current research interests include signal processing, sparse representation, and deep neural network in detail.

XIANG LI received the Ph.D. degree in sparse representation and its application to inverse problem of structural health monitoring (SHM) from the School of Mechanical Engineering, Xi'an Jiaotong University, China, in 2015. He has held post-doctoral research appointment at the Cognitive Science Laboratory, School of Computer Science and Engineering, The University of Aizu, Japan, where he conducted the study of compressive sensing, deep neural network, and non-convex optimization in the inverse problem of Internet of Things (IoT) and SHM. He is currently an Associate Professor with the School of Computer Science and Engineering, The University of Aizu. His main research interests include sparse representation, optimization, machine learning, information theory, and their applications, especially for inverse problems.

SHUXUE DING (M'04) received the M.Sc. degree in physics from the Dalian University of Technology, China, in 1988, and the Ph.D. degree in physics from the Tokyo Institute of Technology, Japan, in 1996.

From 1989 to 1991 and from 1991 to 1992, respectively, he was an Assistant Professor and Associate Professor with the School of Physics and Optoelectronic Technology, Dalian University of Technology. From 1996 to 1998 and from 1998 to 2003, he was with Fujisoft-ABC Inc., and Clarion Co., Ltd., Japan, respectively. From 2003 to 2005, he was a Visiting Faculty, and from 2005 to 2010, he was an Associate Professor with the School of Computer Science and Engineering, The University of Aizu, Japan, where he is currently a Full Professor. He is a member of ACM and IEICE.

Dr. Ding has involved himself in research in a wide range of areas of mathematical and physical engineering, such as statistical signal processing, optimization, neural computation, bioelectromagnetism, and information sciences. In particular, he has devoted himself to compressive sensing and sparse representation, machine learning, brain-style information processing, blind source separation, and independent component analysis. He is also interested in speech and image processing, quantum computation and optimization, quantum information, and other physical theories of information.

LINGJUN ZHAO received the B.Sc. degree from the Department of Civil Engineering, Tangshan University, China, in 2014, and the master's degree from the School of Civil Engineering, Guangzhou University, China, in 2016. She is currently pursuing the Ph.D. degree with the School of Computer Science and Engineering, The University of Aizu, Japan. Her research interests include deep learning, medical image processing, and signal processing.

ZHENNI LI received the B.Sc. degree from the School of Physical Science and Electronics, Shanxi Datong University, China, in 2009, the M.Sc. degree from the School of Physics and Optoelectronic, Dalian University of Technology, China, in 2012, and the Ph.D. degree from the School of Computer Science and Engineering, The University of Aizu, Japan, in 2015. From 2015 to 2017, she was a Visiting Researcher with the School of Computer Science and Engineering, The University of Aizu. She is currently an Associate Professor with the Guangdong Key Laboratory of Internet of Things Information Technology, School of Automation, Guangdong University of Technology, Guangzhou, China. Her research interests include machine learning, signal processing, sparse representation, and quantum computing.